

*Digital Comprehensive Summaries of Uppsala Dissertations
from the Faculty of Pharmacy 395*

Diffusion of model drugs in extracellular matrix mimetic hydrogels

Towards an in vitro model for subcutaneous injection

JULIA PARLOW



ACTA UNIVERSITATIS
UPSALIENSIS
2026

ISSN 1651-6192
ISBN 978-91-513-2706-8
urn:nbn:se:uu:diva-572901



UPPSALA
UNIVERSITET

Dissertation presented at Uppsala University to be publicly examined in B41, BMC, Husargatan 3, Uppsala, Friday, 13 February 2026 at 09:15 for the degree of Doctor of Philosophy (Faculty of Pharmacy). The examination will be conducted in English. Faculty examiner: Senior Lecturer Alain Pluen (Division of Pharmacy & Optometry, School of Health Sciences, University of Manchester, England).

Abstract

Parlow, J. 2026. Diffusion of model drugs in extracellular matrix mimetic hydrogels. Towards an *in vitro* model for subcutaneous injection. *Digital Comprehensive Summaries of Uppsala Dissertations from the Faculty of Pharmacy* 395. 66 pp. Uppsala: Acta Universitatis Upsaliensis. ISBN 978-91-513-2706-8.

Subcutaneous injection is the preferred administration route for degradation-sensitive therapeutic peptides and proteins because it is patient-friendly and can provide sufficient bioavailability. However, both bioavailability and absorption rate vary considerably and are difficult to predict. As yet, no existing *in vitro* model can reliably estimate the pharmacokinetics of new drug compounds, highlighting the need for methods that offer mechanistic insight into transport processes under physiologically relevant conditions.

This thesis investigates the transport properties of model drugs with varying physicochemical properties in hydrogels that mimic the extracellular matrix of subcutaneous tissue. Partitioning and diffusion coefficients were measured in gels and in solution using confocal laser scanning microscopy and fluorescence recovery after photobleaching (FRAP). Experimental results were compared with theoretical models describing obstruction and electrostatic interactions, and the experimentally derived parameters were incorporated into a physiologically based pharmacokinetic (PBPK) model to predict subcutaneous absorption rate and bioavailability.

The results confirm that FRAP enables reliable quantification of local diffusion coefficients in heterogeneous gels. Combined with information on distribution within the gel and gel–solution partitioning, the method provides insight into interactions of the compounds with the gel matrix. Composite collagen–hyaluronic acid gels proved to be the most physiologically relevant, offering appropriate interaction sites along with reproducibility and stability.

Diffusivities in solution depended not only on molecular weight but also on molecular shape and oligomerization. In gels, near-neutral compounds generally showed reduced partitioning and diffusion, whereas highly positively charged peptides and proteins were enriched in polymer-dense regions. This enrichment substantially decreased diffusivity due to obstruction and electrostatic binding. The electrostatic interactions were decreased in the presence of human serum albumin for compounds containing a high-affinity albumin-binding domain, effectively facilitating their transport. Albumin also altered the apparent hydrodynamic size of some molecules by solubilizing oligomers or forming larger complexes.

Finally, it was demonstrated that diffusion and partitioning data from collagen–hyaluronic acid gels correlated with *in vivo* absorption rates of therapeutic proteins and could be used to improve PBPK model predictions. Overall, the presented method offers a valuable characterization tool that can facilitate the design of new drug candidates with predictable pharmacokinetic profiles.

Keywords: diffusion, partitioning, peptides, proteins, extracellular matrix, hydrogel, *in vitro*, subcutaneous, drug delivery, microscopy, FRAP

Julia Parlow, Department of Medicinal Chemistry, Box 574, Uppsala University, SE-75123 Uppsala, Sweden.

© Julia Parlow 2026

ISSN 1651-6192

ISBN 978-91-513-2706-8

URN urn:nbn:se:uu:diva-572901 (<http://urn.kb.se/resolve?urn=urn:nbn:se:uu:diva-572901>)

*The more you read, the more you want to know,
and so the more questions you have.*
- *Xinran*

It goes up, it goes down, and around, and around
C'est la-la-la-la-la vie
- Claude Kiambe

List of Papers

This thesis is based on the following papers, which are referred to in the text by their Roman numerals.

- I. **Parlow, J.**, Rodler, A., Gråsjö, J., Sjögren, H., Hansson, P. (2024) FRAP Analysis of Peptide Diffusion in Extracellular Matrix Mimetic Hydrogels as an *in vitro* Model for Subcutaneous Injection. *International Journal of Pharmaceutics*, 664:124628
- II. **Parlow, J.**, Pet, E., Smirnova, A., Mojumdar, E., Sjögren, H., Hansson, P. (2025) Diffusion of Macromolecules in Extracellular Matrix Mimetic Hydrogels – Effect of Size and Charge. *European Journal of Pharmaceutical Sciences*, 214:107257
- III. **Parlow, J.**, Sandegren, A., Güler, R., Karlberg, I., Frejd, F., Sjögren, H., Hansson, P. (2026) Diffusion of Affibody Molecules in Extracellular Matrix Mimetic Hydrogels and the Effect of Albumin Binding. *International Journal of Biological Macromolecules*, 337:149322
- IV. **Parlow, J.**, Sjögren, E., Al-tikriti, Y., Sjögren, H., Hansson, P. (2025) Diffusion of Therapeutic Proteins in Extracellular Matrix Mimetic Hydrogels – Predicting *in vivo* Absorption after Subcutaneous Injection. *In manuscript*

Reprints were made with permission from the respective publishers.

Contents

Introduction.....	11
Subcutaneous administration route	11
Physiology of the subcutaneous tissue	12
Extracellular matrix.....	13
<i>In vitro</i> models for subcutaneous administration	14
Fluorescence recovery after photo-bleaching.....	16
Aims of the thesis.....	17
Methods	18
Hydrogels	18
Model drugs.....	19
Protein labelling and characterization	20
Dynamic light scattering	22
Partitioning	23
Fluorescence recovery after photobleaching.....	23
Theoretical models	25
Mesh size	25
Partitioning	26
Diffusion.....	27
Physiologically-based Pharmacokinetic Modelling	28
Results and Discussion	30
Gel properties and stability.....	30
Effect of labelling.....	32
Validation of the FRAP method.....	33
Hydrodynamic size.....	34
Partitioning.....	37
Diffusion	40
Agarose gel.....	40
HA-gel	41
COL-HA gel	42
Effects of albumin presence	45
Apparent size	45
Distribution within the gel.....	46
Prediction of <i>in vivo</i> absorption rate.....	47

Main findings	50
Concluding remarks and future perspectives	52
Populärvetenskaplig sammanfattning	54
Populärwissenschaftliche Zusammenfassung	55
Acknowledgements.....	56
References.....	61

Abbreviations

ABD	Albumin-binding domain
CD	Circular dichroism
COL	Collagen type I
COL-HA	Covalently cross-linked collagen and hyaluronic acid gels
D	Diffusion coefficient/diffusivity
$D_{\text{gel}}/D_{\text{sol}}$	Diffusivity of a compound within the gel relative to in solution
DLS	Dynamic light scattering
ECM	Extracellular Matrix
FD	FITC-dextran
FITC	Fluorescein isothiocyanate
FRAP	Fluorescence recovery after photobleaching
GK-peptides	Model peptides with varying number of glycines and lysines
HA	Hyaluronic acid
HSA	Human serum albumin
K	Partition coefficient
Mw	Molecular weight
NMR	Nuclear magnetic resonance
PB model	Electrostatic peptide/protein binding model
PBPK	Physiologically based pharmacokinetics
PBS	Phosphate buffered saline
mAb	Monoclonal antibody
r_h	Hydrodynamic radius
ROI	Region of interest
SC	Subcutaneous
t_{max}	Time to maximum plasma concentration
$t_{90\%}$	Time to 90% of maximum fraction absorbed

Introduction

Subcutaneous administration route

Subcutaneous (SC) injection is a common route of administration for degradation-sensitive drug compounds. One such class of compounds are therapeutic peptides and proteins which include e.g., monoclonal antibodies (mAbs), insulins and protein hormones. Due to limited uptake and sensitivity to degradation, they exhibit poor oral bioavailability. Proteolytic degradation, as well as first pass metabolism are avoided when parenteral routes are used [1]. Compared to the intravenous route, SC administration is often preferred by the patients, since self-administration at the patient's home is possible. This also reduces the cost of the therapy, as fewer appointments with trained health care personnel are needed, which makes it ideal for long-term treatment [2].

However, bioavailability is often incomplete, being in the range of 20-100% and can vary considerably between patients and injection sites [3]. Moreover, the rate of absorption can be highly affected by many factors such as physiological aspects, formulation characteristics, as well as physicochemical properties of the drug compound [4] (Figure 1). Despite increased efforts in recent years to understand the factors affecting the absorption rate and bioavailability of SC drugs, they are still poorly understood. Different animal models are used in early drug development in order to predict the absorption behaviour of drug candidates in humans. However, only few have reliable predictive ability, since there are considerable differences in skin physiology and immune responses between humans and animals [2].

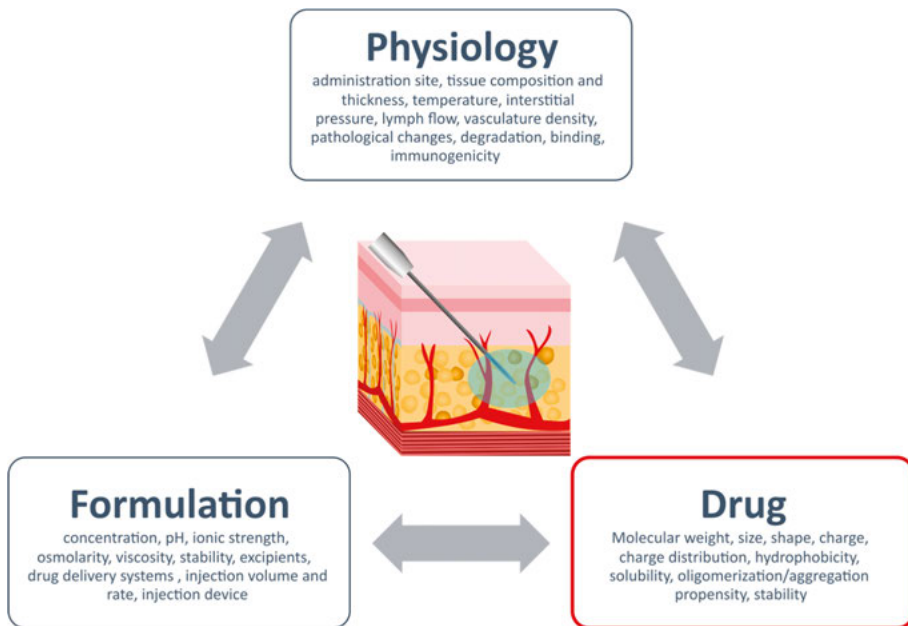


Figure 1. Factors affecting the absorption rate and bioavailability of subcutaneously administered drugs. Figure adapted from [5] and based on references [1,2,4,6].

Physiology of the subcutaneous tissue

From histological and physiological studies [7–9] as well as X-ray tomography studies of SC injection [10], the composition and organisation of the SC tissue as well as the effect of the injection on its integrity can be understood. The SC adipose tissue consists of 90% adipocytes, which have a diameter of 80 μm and are arranged in lobules of 1 mm (Figure 2). The lobules are surrounded by a 10 μm thick open foam like structure composed of collagen fibrils, called the interlobular septa. Within the lobules the adipocytes are enveloped by the 2 μm thick reinforced basement membrane composed of collagen I, III, IV, V and VI. When a drug formulation is injected subcutaneously, it spreads out in the adipose tissue forming minor cracks in the septa in between lobules forming channels of 1 mm width in a 10-15 mm wide region around the injection site.

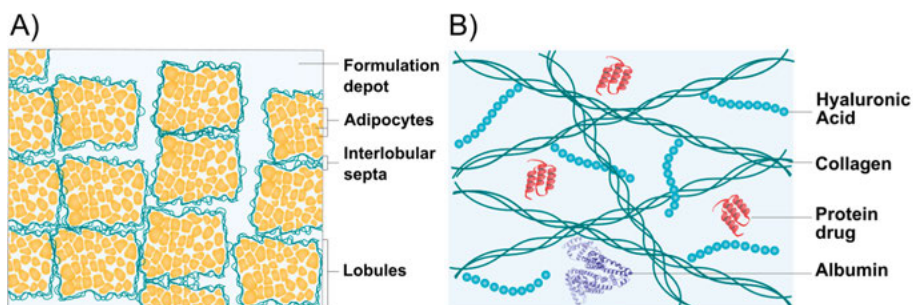


Figure 2. A) Schematic illustration of the subcutaneous tissue depicting adipocytes organized into lobules separated by interlobular septa and microcracks formed after injection. B). Schematic illustration of the extracellular matrix components the injected drug encounters.

For systemic absorption, the drug compound has to be transported from this reservoir to blood capillaries and lymph vessels which are embedded in the extracellular matrix (ECM) of the tissue. Since each adipocyte is served by at least one blood capillary [11], through which small compounds (<10 nm, <16 kDa) can be absorbed, the transport distance for these compounds is in the size range of 10 - 100 μm and can be overcome through passive diffusion. Larger compounds (10 - 100 nm) such as mAbs are mainly absorbed through the lymphatic network [4]. Due to their low diffusivity, their transport is instead heavily affected by the interstitial flow (0.1 - 2 $\mu\text{m/s}$) [12].

Extracellular matrix

As any subcutaneously injected compounds are in close contact with the ECM of the tissue, their transport is likely to be affected by interactions with its different components (Table 1). The biopolymers present in the tissue are, in addition to collagen, also glycosaminoglycans, such as chondroitin sulphate and hyaluronic acid (HA), which are highly negatively charged linear polysaccharides that are solubilized in the interstitial fluid of the tissue [1]. Besides size exclusion effects and obstruction due to the mesh structure of the collagen network, also electrostatic interactions with the glycosaminoglycans, as well as adsorption, can be expected to alter the diffusivities of injected compounds. Furthermore, therapeutic peptides or proteins formulated in a certain buffer at pH and ionic strength suitable for long term storage at 5 $^{\circ}\text{C}$ can oligomerize or aggregate upon injection into physiologic environment (pH 7.4 , 155 mM, 34 $^{\circ}\text{C}$). Drug-drug as well as drug-polymer complex formation would significantly lower the diffusivities of small peptide drugs.

Table 1. The main extracellular matrix (ECM) components and their properties. ^a

ECM component	Charge at pH 7.4	Role in SC tissue	Concentration in SC tissue
Collagen	Positive	Structural	9-17 mg/ml ^b
Hyaluronic acid	Negative	Structural, hydration balance, lubrication, regulation of protein distribution, viscosity modifier	0.5-1.8 mg/ml ^c
Albumin	Negative	Transporter of fatty acids and proteins	4-11 mg/ml ^d

^a table adapted from [1]
References: ^b[13,14], ^c[13-15], ^d[16]

Another important element of the ECM is human serum albumin (HSA), which is the most abundant plasma protein and present in the SC interstitial fluid at relatively high concentrations of 4-11 mg/ml [16]. Due to its physiological role as a carrier of fatty acids and proteins, it can be important for drug absorption after SC injection. In fact, fusion to an albumin-binding domain (ABD) is a well-established strategy to increase the plasma half-life of small peptide/protein drugs that otherwise would be cleared rapidly via renal filtration [17,18].

In order to understand interactions and effects possibly influencing the transport through the tissue and thereby the absorption of subcutaneously administered drugs, there is a need for new physiologically relevant *in vitro* models. These would be valuable tools in the early drug development of new drug candidates, potentially decreasing the amount of animal experiments and facilitating the development of new therapeutics for currently unmet medical needs.

In vitro models for subcutaneous administration

In recent years, *in vitro* models with varying degree of complexity have been developed, aiming to predict the *in vivo* performance of subcutaneously injected drugs. Most complex is the *ex vivo* system Hyposkin [19], which makes use of human skin biopsies from abdominal surgery. Formulations can be tested via injection into the hypodermis of the sample and the absorption is measured continuously as the concentration increases in the acceptor compartment. This method is rather complicated and costly and because several factors can contribute to the observed absorption, no detailed mechanistic insight into the effects of individual components can be gained.

Another commercially available method is the SCISSOR system (Subcutaneous Injection Site Simulator), which is based on dialysis [20]. When evaluating a formulation in the SCISSOR system, the formulation of interest is injected into a dialysis chamber containing high molecular weight HA.

Thereafter, the light transmittance in the cartridge as well as the concentration profile in the surrounding sink solution are measured over time. In this way, precipitation, dissolution and release of the drug from the formulation as well as the transport of the drug through the HA solution can be investigated. This system has been shown to be able to predict the bioavailability of a set of mAbs [3] and has also been evaluated for smaller peptide drugs [21]. Limitations have been the stability of the HA inside the dialysis chamber as well as sticking of the investigated drug compounds to the tubing in the SCISSOR system. Lately, this system has been developed further to even include collagen [22].

A variety of hydrogel based systems composed of collagen and HA have been developed [23–25] while other approaches focus on size exclusion effects of the ECM polymer network using Sephadex or agarose gels [26–28]. Some of the methods were able to capture the rank order of different commercially available formulations of insulin. Other research groups have focused on the composition of the interstitial fluid [29], and yet others aim to elucidate the effect of the lymphatic absorption using an on-chip lymphatics model as a tool for rank ordering SC lymphatic absorption [30]. In addition to *in vitro* methods, *in silico* approaches have been developed to model the pharmacokinetics of subcutaneously injected drugs [5,31–33]. Despite these increased efforts and emerging tools for investigating factors affecting drug absorption after SC injection, no single *in vitro* method has been sufficient to reliably predict the bioavailability of a wide range of drug compounds intended for SC administration [34,35].

In parallel, in our lab, an ECM mimetic hydrogel composed of crosslinked collagen type I (COL) and HA has been developed and characterized [36]. The composite COL-HA gels represent a physiologically relevant environment since they resemble concentrations of COL and HA as in the biological tissue as well as mechanical properties mimicking the ECM of the tissue. In addition to obstruction effects and electrostatic interactions with negatively charged HA, collagen fibres serve as a site for nonspecific adsorption. Furthermore, the heterogeneous nature of the gel reflects the heterogeneity of the biological tissue [37–39], with polymer-rich regions adjacent to regions of low polymer concentration, where the movement of larger molecules and cells is less restricted.

Because the hydrogel is covalently crosslinked, it is mechanically stable and can be cast into molds of any size. Its composition is controllable and tuneable, which could be beneficial when aiming to mimic different injection sites or pathological changes of the tissue properties. The model is relatively simple containing only two components, which makes it possible to

understand the contributions of the different constituents. However, complexity can be increased by incorporating additional components, e.g., HSA.

Fluorescence recovery after photo-bleaching

Fluorescence recovery after photo-bleaching (FRAP) is a versatile tool for measurement of local as well as global diffusivities in heterogeneous hydrogels at the micrometre scale [40]. In general, a spot within the gel is imaged at low laser intensity in order to minimize the photobleaching during image acquisition. At time zero, the laser intensity is increased when scanning a pre-determined region of interest (ROI), irreversibly bleaching a fraction of the fluorescent molecules present in the ROI at that time. The recovery of the fluorescence intensity within the ROI is then monitored over time, as non-bleached molecules from the surroundings enter and bleached molecules diffuse out of the spot. From the resulting recovery curve, the self-diffusion coefficient can be extracted using mathematical models. If all fluorescent molecules are mobile, the fluorescence intensity will recover completely. Incomplete recovery, on the other hand, indicates the presence of an immobile fraction being “trapped” or bound within the spot in the gel [41].

Since the first FRAP experiments conducted in the 1970s [42,43], this method has been used extensively in cell biology, pharmaceutical and food science, and has been developed considerably in order to be more suitable for quantitative determination in various challenging conditions. Computational FRAP methods are all based on their own specific assumptions and range from very simple empirical methods describing the recovery with a simple exponential function [44] to closed form models based on theoretical descriptions of the full FRAP process [45].

All-pixel based models, such as the rectangle FRAP method (rFRAP) published by Deschout *et al.* [46] even take into account all available spatial and temporal information of the image stack, yielding more accurate values of the diffusion coefficient. Since the microscope’s effective photobleaching and imaging resolution is included in the free fitting parameter, the bleached rectangle can have any size and aspect ratio, and diffusion during bleaching can be compensated. Therefore, the rFRAP model, as one of the most flexible and practical methods for quantitative FRAP analysis, is well suited for determination of self-diffusion coefficients of relatively fast diffusing probes, e.g., proteins and peptides within heterogeneous materials such as ECM mimetic hydrogels.

Aims of the thesis

The objective of this thesis was to investigate **physicochemical aspects** of the absorption of drug molecules, in particular **therapeutic peptides and proteins**, after **subcutaneous administration**. The **partition** and **diffusion** coefficients of model drugs with varying properties (size, charge, oligomerization propensity, glycosylation degree) were determined in **solution** and in **hydrogels** mimicking the **extracellular matrix** of the tissue. The aim was to elucidate the contribution of **obstruction effects, size-exclusion, electrostatic interactions** as well as **drug-drug** and **drug-polyelectrolyte complex** formation to the transport properties of the tested compounds. Furthermore, the effect of the presence of **albumin** was investigated with special emphasis on Affibody molecules containing an **albumin-binding domain**. Ultimately, the goal was to develop an ***in vitro* method** to improve predictions of *in vivo* drug **absorption kinetics** after subcutaneous injection.

Methods

Hydrogels

Three different types of gels were used to evaluate the contribution of different interactions with the gel matrix affecting the diffusivities of the model drugs. Agarose (1%) gel was chosen as a neutral loose gel network reflecting merely the obstruction effects of the polymer network. HA gels (2%) are highly negatively charged and were chosen to, in addition to obstruction effects, elucidate the contribution of electrostatic interactions to the observed diffusivities.

HA (200 kDa) was chemically modified according to the protocol presented by Shu *et al.* [47]., which was adapted with the aim to attach a free thiol-group to 20-30% of the carboxylic acid moieties of the polymer (Figure 3A). The degree of modification was determined with Ellman's test [48] and ^1H NMR [47]. Rat tail collagen type I was modified according to the protocol by Ravichandran *et al.* [49], aiming for methacryloyl-functionalization of approximately 70% of the free amines of lysine and arginine residues within the protein (Figure 3B). The degree of modification was determined with a colorimetric assay [50] and ^1H NMR [49].

For the fabrication of the mixed COL-HA gels, the modified polymer-precursors were cross-linked through Thiol-Michael Addition click-reaction [51]. For that, the freeze-dried precursors were dissolved in N_2 -flushed water and mixed together with the photo-initiator. The mixture was cast into molds of 4 mm or 8 mm diameter for microscopy studies and rheology characterization, respectively, and crosslinked under ultraviolet light.

HA gels were made from 2% solutions of the thiol-modified HA in N_2 -flushed water, cast into molds as above and crosslinked through oxidation and formation of disulphide bridges at pH 9 when exposed to air. Agarose gels were made from 1% agarose solution in phosphate buffered saline (PBS), which formed a gel after heating to 80 °C, casting into molds as above, and cooling to room temperature. All gels were washed and equilibrated in PBS before they were used either for microscopy studies or for viscoelastic characterization with rheology. To confirm successful crosslinking and evaluate the mechanical properties of the gels, the storage G' and the loss G'' moduli were determined at varying oscillation strain and at varying oscillation frequency as reported previously [52].

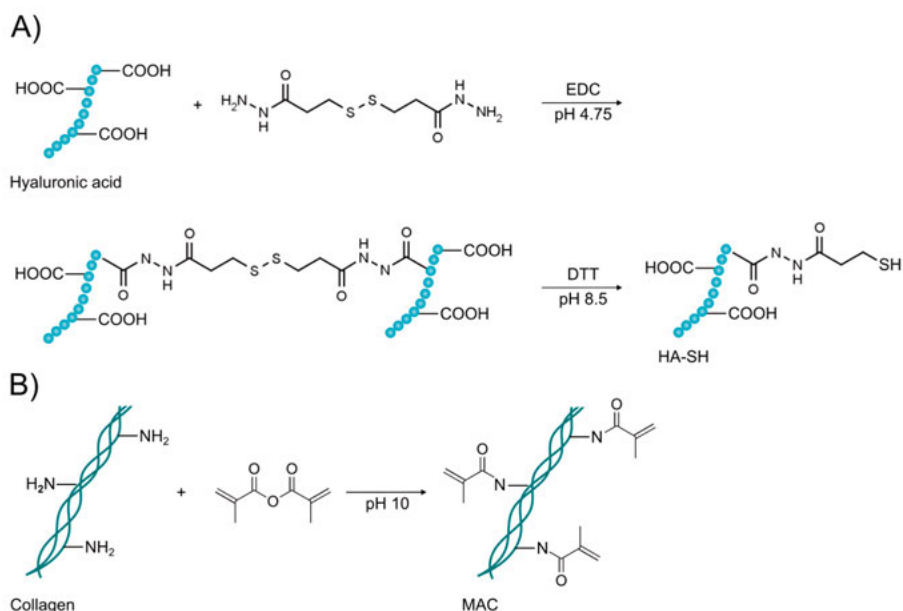


Figure 3. Synthesis of thiol-modified hyaluronic acid (HA-SH) (A) and methacryloyl-functionalized collagen (MAC) (B).

Model drugs

Model drugs were chosen to systematically vary in their physicochemical properties (Table 2). In project I model drugs of approximately the same size (3-4 kDa) with rather extreme differences in net charge (+20, -20 and neutral) were chosen in order to demonstrate the method's capability to detect electrostatic interactions within the gels in terms of altered diffusivity. Also, the GLP-1 analogue exenatide, a 39 amino acid therapeutic peptide (net charge - 2) used for treatment of diabetes, was included as an example of a subcutaneously administered drug.

In project II, the effect of size and charge on the diffusion within the gels was investigated, using FITC-dextran (FD) of varying sizes (4-150 kDa) as well as small synthetic peptides (2 kDa) composed of different ratios of glycines and lysines (GK-peptides) resulting in varying number of positive charges (+2, +3, +5, +9).

In project III, the transport properties of a set of HER2/HER3-targeting Affibody molecules were investigated. The Affibody molecules represent a class of small protein ligands (7-19 kDa) with similar subdomain structure and target-binding affinity but varying in size, charge, and HSA-binding propensity. In addition, HSA and the mAb trastuzumab (Herceptin) were included as reference.

In project IV, therapeutic proteins intended for SC administration were chosen, covering a wide range of physicochemical properties and reported *in vivo* absorption rates. These included the most common classes of SC pharmaceuticals, insulins and mAbs, as well as protein hormones somatropin and follitropin, and the biologic fusion protein etanercept.

Protein labelling and characterization

The peptides and proteins used in projects I, III, and IV were labelled with amine-reactive fluorescein isothiocyanate (FITC) according to the standard protocol [53]. Since reactive primary amines are present at the N-terminus as well as at the lysine side chains of the peptides and proteins, multiple labelling can occur. However, the reaction can be directed primarily towards the N-terminus by controlling pH, reaction time, and FITC:peptide/protein molar ratio. Multiple labelling can, in addition to the overall size, charge, and hydrophobicity of the molecule, potentially alter its secondary structure and aggregation propensity, and cause fluorescence quenching. Therefore, mono-labelled products are preferable, and the product should be characterized post-labelling.

The labelled peptides/proteins were purified through gel filtration, and the concentration of the product was determined from absorbance measurements at 280 nm and 495 nm. The degree of labelling was then calculated as the ratio of labelled and unlabelled peptide/protein concentrations (F/P ratio). For exenatide, insulins, Affibody molecules, and somatropin, the purity and number of attached dye-molecules were determined with analytical high performance liquid chromatography and mass spectrometry (HPLC-MS).

In order to understand the effect of labelling on the apparent hydrodynamic size of the molecules as well as their secondary structure, dynamic light scattering (DLS) and circular dichroism spectroscopy (CD) were carried out for labelled and unlabelled equivalents of some of the tested molecules (GK-peptides, Affibody molecules ZZA and 3A3, HSA, Herceptin).

Table 2. The tested model drugs and their properties.

Model drug	Format	Mw (kDa)	Net charge ^a	Paper
PLK20	Poly(L-lysine hydrobromide) 17-23 amino acids	2.2-3.0	+20	I
PLE20	Poly(L-glutamic acid sodium salt) 17-23 amino acids	2.2-3.0	-20	I
Exenatide	GLP-1 analogue, 39 amino acids	4.2	-2	I
FD4	FITC-dextran (0.007 mol FITC/glucose)	4	-0.2	I, II
FD10	FITC-dextran (0.011 mol FITC/glucose)	10	-0.6	II
FD40	FITC-dextran (0.005 mol FITC/glucose)	37	-1.0	II
FD70	FITC-dextran (0.013 mol FITC/glucose)	66	-4.8	II
FD150	FITC-dextran (0.005 mol FITC/glucose)	149	-4.2	II
GK3	FITC-Ahx-GW[KGGGGG] ₃ -NH ₂	2.0	+2	II
GK4	FITC-Ahx-KWGGG[KGGGG] ₃ -NH ₂	2.1	+3	II
GK6	FITC-Ahx-GW[KGG] ₆ -NH ₂	2.2	+5	II
GK10	FITC-Ahx-KW[KG] ₉ -NH ₂	2.5	+9	II
2	HER2-targeting Affibody molecule target-binding domain	7.6	+1	III
2A	HER2-targeting Affibody molecule target-binding domain and ABD	12.5	-1	III
ZZA	HMGB1-targeting Affibody molecule 2 target-binding domains and 1 ABD	19.2	-12	III
3	HER3-targeting Affibody molecule target-binding domain	7.4	0	III
3A	HER3-targeting Affibody molecule target-binding domain and ABD	12.0	+3	III
3A3	HER3-targeting Affibody molecule 2 target-binding domains and 1 ABD	19.0	+4	III
HSA	Human serum albumin	66.4	-19	III
Herceptin (trastuzumab)	Monoclonal antibody, HER2-targeting	145.5	+5.3	III
Insulin aspart	Rapid-acting insulin, Aspartic acid at position B28, increased solubility and decreased propensity to self-associate	5.8	-3.8	IV
Insulin human	Regular human insulin, present as monomers, dimers and hexamers	5.8	-2.8	IV
Insulin detemir	Acylation at Lysine B29, reversible binding to albumin	5.9	-3.8	IV
Somatropin	Human growth hormone	22.1	-6.1	IV
Follitropin delta	Follicle stimulating hormone, glycosylation pattern with high sialic acid content	33.7	-1.1	IV
Etanercept	Dimeric fusion protein, anti-TNF, complex glycosylation profile	150	-4.9	IV
Adalimumab	Monoclonal antibody, Anti-TNF	144	+5.3	IV
Denosumab	Monoclonal antibody, RANKL inhibitor	145	+8.6	IV
NISTmAb	Monoclonal antibody, reference material for characterization methods	150	+6.9	IV

^aEstimated theoretical net charge at pH 7.4

Dynamic light scattering

DLS is commonly used to determine particle sizes in solutions, suspensions, and emulsions. In DLS, the sample is illuminated with a monochromatic coherent light source and the scattered light is recorded at a fixed angle. As the particles in solution move relative to each other due to Brownian motion, the frequency of the scattered light is shifted, causing a distribution of frequency shifts over time, which can be determined in comparison to a coherent optical reference. The optical reference can either be provided by the scattered light itself (homodyne detection) or by a controlled reference (heterodyne detection) [54] (Figure 4). In both methods, the distribution of frequencies is used to extract the size of the particles. The evaluation of the signal can be done using a time-dependent autocorrelation function or a frequency power spectrum (FPS). Autocorrelation determines the average intensity based mean size, and a polydispersity index and curve fitting algorithms are required to estimate the particle size distribution. FPS, on the other hand, provides a more direct measure of the size distribution [55].

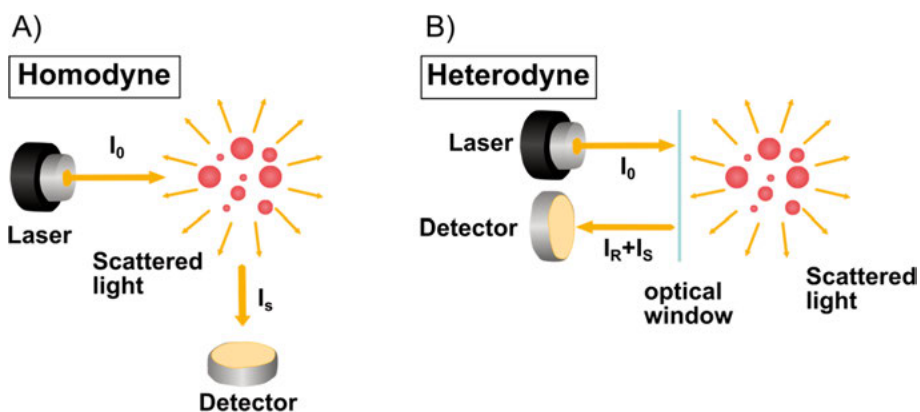


Figure 4. Schematic illustration of homodyne (A) and heterodyne (B) systems for dynamic light scattering adapted from [54,55]. In heterodyne detection, in addition to scattered light (I_s) also reference light (I_R) reaches the detector.

Since heterodyne detection in combination with FPS provides a stronger signal and enables the detection of multimodal distributions, it is especially useful for small and low-scattering particles such as the peptides and proteins investigated in this work. However, all DLS methods require sufficient concentrations and scattering properties of the particles. Moreover, the hydrodynamic radius (r_h) obtained from DLS reflects the size of a spherical particle with the same diffusivity as the particle in the sample. In order to get an idea of the real dimensions of the particle, additional information about its shape is required.

Partitioning

The solutions of FITC-labelled peptides/proteins were diluted to give concentrations as low as possible to avoid aggregation/precipitation and fluorescence quenching while ensuring sufficient fluorescence signal. The gels were placed directly in the wells of a chambered microscope slide and equilibrated in the peptide/protein solutions. In papers II and IV, the partition coefficients (K) were determined as the ratio of the mean fluorescence intensity within the gel and in the surrounding solution. The gel-solution interface was imaged 100 μm into the sample with a confocal laser scanning microscope. Mean intensities of representative ROIs within the gel and the solution were defined and analysed using Fiji image analysis software [56]. In paper III, this was done in an automated process instead, defining the partition coefficient as the ratio of mean intensity in high intensity regions and low intensity regions identified via automatic thresholding.

Fluorescence recovery after photobleaching

For FRAP experiments, the fluorescently labelled compounds were introduced into the gels via passive diffusion in order to avoid trapping within the voids of the polymer networks. The gels were immersed in solutions of the labelled peptides directly in the wells of the chambered microscope slide and equilibrated for at least 48 hours. For determination of the self-diffusion coefficients in solution, 5 μl of the solution was placed on a microscope slide prepared with a 120 μm double adhesive spacer forming wells of 9 mm diameter and sealed with a cover slip. In this way, self-diffusion coefficients in a 3D extended sample could be determined while avoiding any interference of convection.

The FRAP experiments were performed 50-100 μm into the gel or solution droplet using a 10x objective lens with low numerical aperture. For imaging, a 488 nm argon laser was used at low intensity and the gain adjusted to achieve high signal without oversaturated pixels. A square-shaped ROI (20-100 μm) was placed in the middle-left region of a 250-500 μm frame. A reference region of similar size was chosen sufficiently far from the bleached ROI not to be affected by the diffusion front. After recording 3 pre-bleach images, the spot was bleached at high laser intensity for repeated iterations until the mean intensity in the bleach ROI had dropped to 70-90% of the original value. Thereafter, the fluorescence recovery was recorded in 50-100 frames acquired at a fast scan rate (0.06-0.3 s per frame).

For image analysis, each frame was cropped to the ROI dimensions, extended by 10 pixels on all sides. Pixel intensities were subsequently double-

normalized: first to the pre-bleaching intensity and then to the intensity of the reference region.

$$F(x, y, t) = \frac{ROI}{ROI_{pre}} \times \frac{Ref_{pre}}{Ref} \quad (1)$$

where ROI is the intensity within the bleached region at each time point and pixel, ROI_{pre} is the intensity in the bleached region before the bleaching event, Ref is the mean intensity in the reference region, and Ref_{pre} is the mean intensity in the reference region before the bleaching event.

The double normalized intensity values for each pixel at each time point, $F(x,y,t)$, were simultaneously fitted with a least-squares fit in Matlab according to the following equation:

$$F(x, y, t) = \phi_{mob} \left\{ 1 - \frac{K_0}{4} \left[\operatorname{erf} \left(\frac{x + \frac{l_x}{2}}{\sqrt{r^2 + 4Dt}} \right) - \operatorname{erf} \left(\frac{x - \frac{l_x}{2}}{\sqrt{r^2 + 4Dt}} \right) \right] \times \left[\operatorname{erf} \left(\frac{y + \frac{l_y}{2}}{\sqrt{r^2 + 4Dt}} \right) - \operatorname{erf} \left(\frac{y - \frac{l_y}{2}}{\sqrt{r^2 + 4Dt}} \right) \right] \right\} + (1 - \phi_{mob}) \times (1 - K_0 \times F_{BL}) \quad (2)$$

where ϕ_{mob} is the fraction of mobile molecules, K_0 is the degree of photo-bleaching, l_x is the length of the bleached region in the x-direction, l_y is the width of the bleached region in the y-direction, r^2 is the effective resolution parameter, and D is the diffusion coefficient. F_{BL} is the fraction of bleached and bound molecules and is defined as follows:

$$F_{BL}(x, y, t) = \begin{cases} 1 & \text{if } -l_x/2 \leq x \leq l_x/2 \text{ and } -l_y/2 \leq y \leq l_y/2 \\ 0 & \text{otherwise} \end{cases} \quad (3)$$

The free fitting parameters in this case are D , K_0 , and r_2 . Representative images indicating the placement of the ROI and the reference region, as well as examples of y-plots of the intensities at a fixed x-value over time are shown in 5.

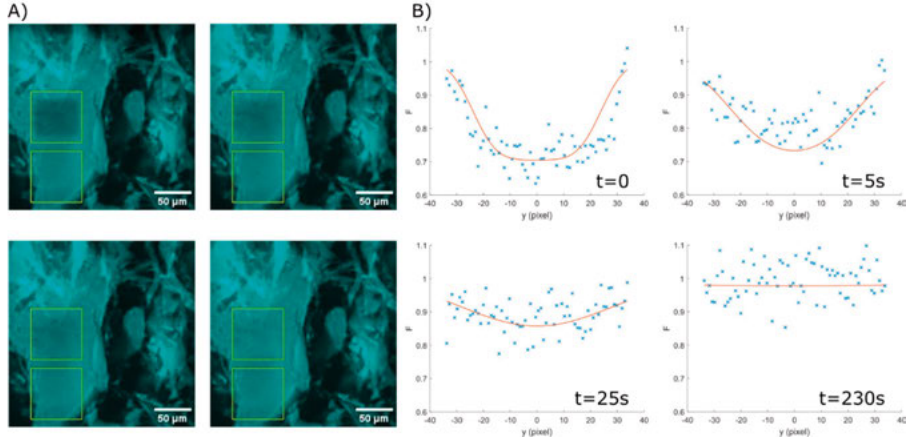


Figure 5. rFRAP experiment for FITC-PLK20 in COL-HA gels. (A) Representative images (256x256 pixels) showing the bleach moment ($t = 0$) and the recovery at time points 5 s, 25 s and 230 s. A region with the size of the bleached square ($50 \times 50 \mu\text{m}$) extended by 10 pixels is used for analysis (yellow box). The bleached region is placed within a high-intensity domain of the inhomogeneous gel and the reference region (yellow box) is placed in a region of similar pre-bleach intensity, which is sufficiently far from the bleached spot. For visual representation of the quality of the fit, the normalized intensity (F) in each pixel at a certain y -value in the middle of the analysis region is depicted at the same time points in (B).

The rFRAP model was validated with a series of measurements of FD4 in sucrose solutions of varying viscosities in order to evaluate the agreement of the resulting values with the theoretical values calculated from the Stokes-Einstein equation:

$$D = \frac{k_B T}{6\pi\eta r_h} \quad (4)$$

where k_B is Boltzmann's constant, T is the absolute temperature, η is the viscosity, and r_h is the hydrodynamic radius of the diffusing particle. In addition, the sensitivity of the method when changing spot size or using different microscopes was assessed.

Theoretical models

Mesh size

Many of the models describing the hindrance of the gel network for the diffusion of a solute depending on its size, build on a reliable estimate of the hydrogel mesh size. One way to describe mesh size, which is compatible with several different models giving accurate predictions of diffusivities in

hydrogels, is the correlation length, ξ , [57]. For weakly charged polymer networks in the presence of salt, it is defined as:

$$\xi = R_g \left(\frac{c^*}{c} \right)^{0.76} \quad (5)$$

where R_g is the radius of gyration and c^*/c is the ratio between the overlap concentration and the actual polymer concentration. For the mixed COL-HA gel eq. (5) has to be adapted to represent the mixture of polymers, resulting in the following equation introduced in paper II [58]:

$$\xi = (x_{HA}R_{g,HA} + x_{COL}R_{g,COL}) \left(\frac{(c_{HA}^* + c_{COL}^*)}{(c_{HA} + c_{COL})} \right)^{0.76} \quad (6)$$

where x_{HA} and x_{COL} are the mole fractions of HA and COL chains, respectively, and c_{HA}^* and c_{COL}^* are the concentrations of HA and COL, respectively, at the overlap concentration for the mixture with the same molar ratio of HA and COL as in the gel.

Partitioning

Ogston model

Regarding the gel network as an array of randomly oriented cylindrical fibres, the partition coefficient, K , of uncharged spherical macromolecules between a hydrogel and the surrounding solution can be described by the Ogston model [59,60]:

$$K = \exp \left[-\Phi \left(1 + \frac{r_h}{r_f} \right)^2 \right] \quad (7)$$

where Φ is the volume fraction of polymer fibres, r_h is the hydrodynamic radius of the sphere, and r_f is the radius of the polymer fibres.

PB model

In order to predict the partition coefficient of the highly positively charged peptides/proteins in the oppositely charged polyelectrolyte gels, electrostatic interactions have to be considered as well. In the electrostatic peptide/protein binding model (PB model) presented in paper II [58], the contribution of the electrostatic binding to the partition coefficient, K_{PB} , for a peptide/protein of charge, z , is described as follows:

$$K_{PB} = \exp\left(-\frac{zF\Delta\psi_1}{RT}\right) \quad (8)$$

where F is the Faraday's constant, R is the ideal gas constant, T is the absolute temperature, and $\Delta\psi_1$ is the difference in mean electrostatic potential between the polymer-rich domain and the liquid which can be calculated for a cell reflecting the total composition of the polyelectrolyte system using the "PB cell" software [61].

Diffusion

Obstruction model

The obstruction model derived by Amsden [57,62] is based on the Ogston expression for the distribution of spherical spaces between randomly oriented linear fibres and describes the effect of increased path length for the diffusing solute due to the presence of impenetrable obstacles. It relates the relative diffusion coefficient within the gels compared to the diffusion coefficient in solution, D_{gel}/D_{sol} , to the solute size, r_h , the polymer fibre radius, r_f , and the hydrogel mesh size expressed as correlation length, ζ (eq. (5) or (6)), as follows:

$$\frac{D_{gel}}{D_{sol}} = \exp\left[-\pi\left(\frac{r_h+r_f}{\zeta+2r_f}\right)^2\right] \quad (9)$$

The predictions of the obstruction model in combination with the correlation length as measure of mesh size have been shown to give reliable estimates of D_{gel}/D_{sol} for molecules over a wide range of hydrodynamic radii (0.15-2.9 nm) and hydrogel mesh sizes (1-11 nm) [57].

Hydrodynamic model

The semiempirical hydrodynamic model derived by Cukier [63] and developed by Fujiyabu *et al.* [64] is a somewhat simpler expression describing the decrease of the diffusivity in the hydrogel as a result of enhanced frictional drag in the proximity to the polymer chains. Making use of the correlation length as measure of mesh size, ζ , and the hydrodynamic diameter of the solute, d_h , the expression:

$$\frac{D_{gel}}{D_{sol}} = \exp\left(-\frac{d_h}{\zeta}\right) \quad (10)$$

has been shown to provide predictions of D_{gel}/D_{sol} with good agreement with experimental data, similar to the obstruction model [57].

PB model

Both the obstruction model and the hydrodynamic model are only valid for uncharged spherical molecules. In order to take into account also electrostatic interactions, the PB model presented in paper II [58] can be used. It describes the contribution of electrostatic interactions to the overall, $(D_{gel}/D_{sol})_{PB}$, depending on the net charge, z , of the peptide/protein as follows:

$$\left(\frac{D_{gel}}{D_{sol}}\right)_{PB} = \frac{1}{1+\hat{r}hk^z} \quad (11)$$

where \hat{r} is a geometrical factor for the relative size of the domains surrounding the polymer chains containing bound molecules, and k is the ratio of concentrations of positive charges in respectively the bound, C^b_+ , and free, C^f_+ , domains, both obtained from solutions of the Poisson-Boltzmann equation in cylindrical geometry by means of the software “PB cell” developed by Bengt Jönsson, Lund University [61]. The correction factor h is introduced to correct for the competitive binding of peptide/protein and sodium ions to HA and was estimated from curve fitting of data in paper II to be 0.64 for COL-HA gels and 0.48 for HA gels.

Physiologically-based Pharmacokinetic Modelling

In silico mechanistic mathematical models, such as physiologically-based pharmacokinetic (PBPK) models, can be used to describe and predict SC drug absorption. Integrating mechanistic knowledge of anatomy, physiology and drug disposition, PBPK models predict the drug concentrations in plasma, lymphatics and different tissues [65]. In many models describing the absorption of therapeutic peptides and proteins, administration and organ compartments are divided into vascular and interstitial sub-compartments, in which the transport is governed by both convection and diffusion [5]. Absorption is often described using the two-pores formalism [66], in which a large number of small pores (~ 9 nm) and a smaller number of large pores (~ 50 nm) represent the available connection between the interstitial space and plasma.

The PBPK model used in this work is illustrated schematically in Figure 6. It describes the injection site as the formulation depot of a certain volume surrounded by interstitial tissue layers with discrete thickness. Upon injection 50% of the injected volume will disperse directly into the adjacent tissue layers, whereas the rest remains in the cylinder-shaped depot. Thereafter the drug distributes to the different layers over time as a result of passive diffusion. In each layer, drainage to the plasma and the lymphatics is represented. In

addition, uptake into cells can occur, where endosomal functionalities (e.g., degradation, FcRn-recycling) are present. The sum of all processes results in simulations of the total absorption profile and bioavailability. For comparison to literature data, the maximum value at the absorption plateau was regarded as a prediction of bioavailability, and the time to reach 90% absorption ($t_{90\%}$) was used as a measure of absorption rate to compare to the time to maximum plasma concentration (t_{max}). Simulations were done either with default settings in which the size and the diffusion coefficient of the compound were predicted from its molecular weight, or using the size and diffusion coefficient determined experimentally.

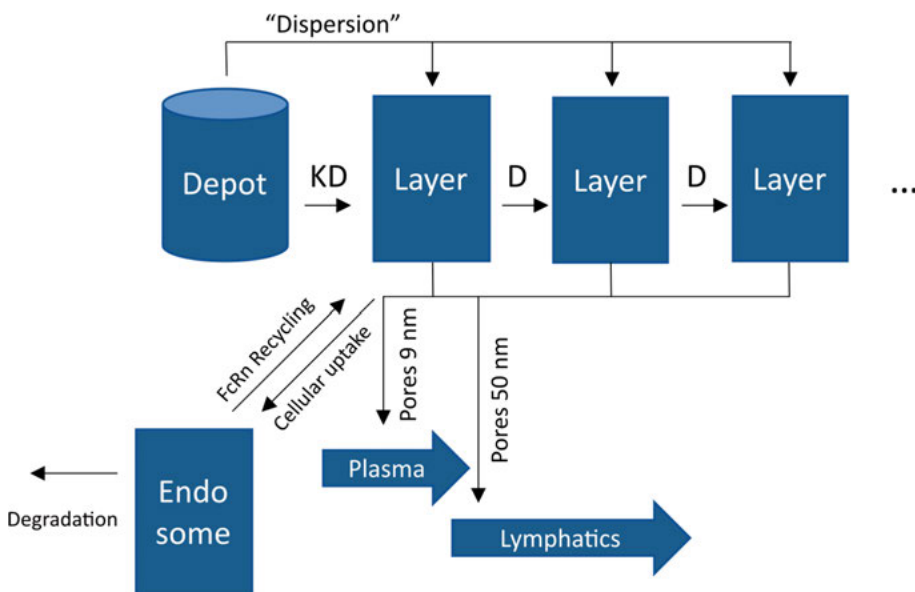


Figure 6. Schematic illustration of the PBPK model.

Results and Discussion

Gel properties and stability

After casting, all gels were firm and transparent (Figure 7A), maintaining their shape upon equilibration in PBS buffer containing 0.02% NaN₃. The mechanical properties of COL-HA gels in terms of the storage modulus G' were evaluated directly after fabrication and at several time points of storage, in order to confirm successful crosslinking as well as stability of the gel. When storing the gels in PBS buffer with 0.02% NaN₃ at 5 °C, the storage modulus G' of COL-HA gels remained unchanged over at least 8 months, indicating that the gels are mechanically stable for that time period (Figure 7B).

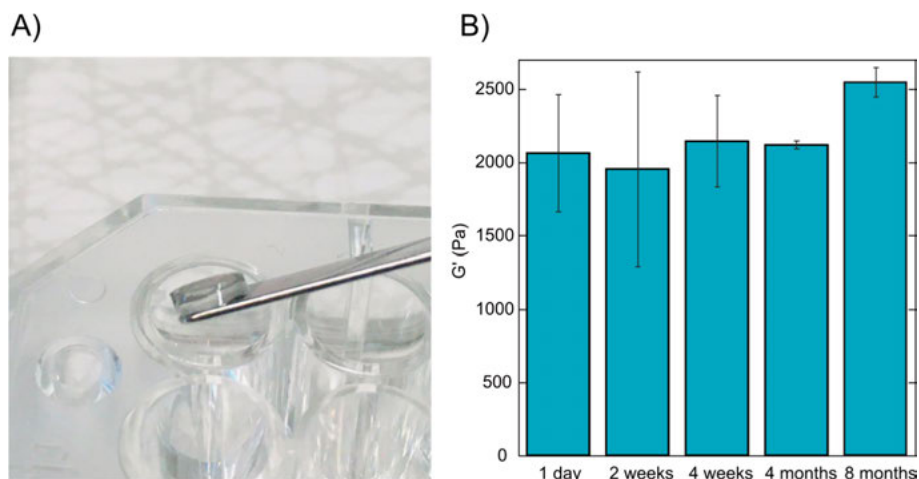


Figure 7. A) COL-HA gel (4 mm diameter) after casting and equilibration in PBS. B) Storage modulus G' of COL-HA gels (8 mm diameter) after different storage times in PBS with 0.02% NaN₃. Shown are the average and standard deviation of 3 gels at each time point.

The fabrication of HA gels was less robust, resulting in larger variation of G' between batches (1822 ± 1078 Pa), which decreased considerably after 1-2 weeks of storage (277 ± 216 Pa). Moreover, HA gels were shrinking over time, indicating rearrangement of the cross-links, resulting in changes in the microstructure of the gel network. Although studies in gels merely consisting of HA can contribute insights about interactions with this particular component of

the ECM, the stability issues along with the relatively high HA concentration (2%) and dense structure compared to biological tissue, make this gel type less suitable as a model of the ECM. Therefore, studies were limited to COL-HA gels and neutral Agarose gels as control in projects III and IV.

Another interesting feature of the COL-HA gels is that they exhibit a rather heterogeneous microstructure with polymer-rich regions interspaced with polymer-lean regions, which can be seen in images of the gels in which the autofluorescence of COL is recorded (Figure 8A). In microscopy images of COL-HA gels immersed in FD500 (Figure 8B), the relatively large FD500 ($r_h \approx 14$ nm) is effectively excluded from the denser regions, which appear as dark structures interrupted by channels of high intensity, where FD500 can enter freely. From these images, the fraction of the dense polymer-rich regions was estimated to be ~ 0.5 . Hence, assuming for simplicity that the polymer concentration in the polymer-lean regions is ~ 0 , the effective concentration within the polymer-rich regions can be estimated as double the average concentration. From that, an estimate of the mesh size within the polymer-rich regions can be calculated using eq. (2).

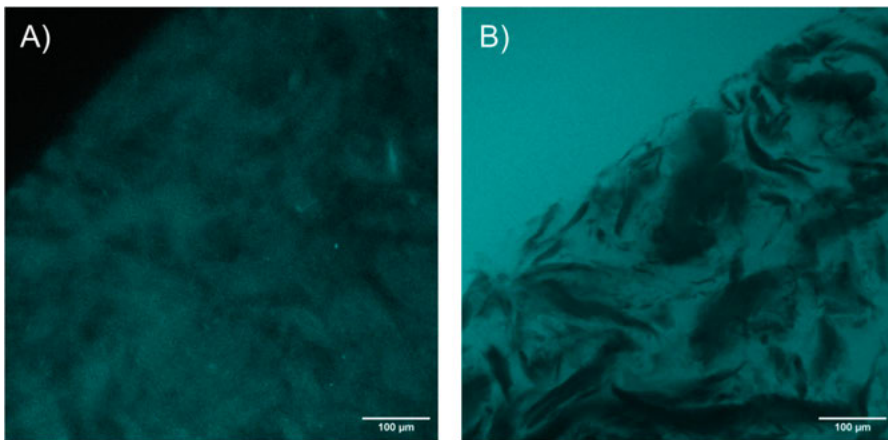


Figure 8. Confocal microscopy images ($640 \times 640 \mu\text{m}$) of COL-HA gels at the interface to the surrounding solution indicate the presence of polymer-rich and polymer-lean domains. Recordings of collagen's autofluorescence A) show polymer-rich and polymer-lean regions. The bright structures in B) originate from FITC-dextran (500 kDa) filling the voids in between the polymer-rich domains.

In Table 3, the properties of the gels in terms of G' , mesh size, polymer concentration, polymer fibre radius, and polymer volume fractions are summarized.

Table 3. Properties of the tested gels.

	Agarose	HA	COL-HA
G' (Pa)^a	8906±920	1822±1078	1914±261
Mesh size (nm)^b			
Average	20 ^c	4.9	8.3 ^d (8.6 ^e)
Polymer-rich domains			4.9 ^d (5.1 ^e)
Polymer concentrations (%)			
Average	1	2	COL: 0.8 HA: 0.16 ^d (0.12 ^e)
Polymer-rich domains	-	-	COL: 1.6 HA: 0.3 ^d (0.24 ^e)
Polymer volume fraction	0.0098	0.011	0.0070 ^d (0.0068 ^e)
Polymer fibre radius (nm)	1.9	0.4	0.69 ^d (0.70 ^e)

^a Data are presented as average ± standard deviation of measurements in 6, 39 and 9 gels of Agarose, COL-HA and HA respectively.

^b calculated using eqs. (5) and (6)

^c chosen to fit data from FD diffusion experiments

^d gels in paper I, II, IV

^e gels in paper III

Effect of labelling

The effect of FITC-labelling on the properties of the peptides/proteins was evaluated in terms of hydrodynamic radius determined with DLS and secondary structure determined with CD of labelled and unlabelled equivalents for some of the model compounds. DLS measurements showed a small increase in hydrodynamic radii for the labelled versions of HSA and GK-peptides GK3, GK4 and GK6, whereas labelled Affibody molecule ZZA appeared smaller than the unlabelled equivalent (Table 4). For labelled GK10, on the other hand, larger particles were detected (222±99 nm), indicating the formation of aggregates at the studied experimental conditions (155 mM PBS pH 7.4, conc. 10 mg/ml). However, it should be noted that for DLS measurements, relatively high concentrations are needed (10 mg/ml). Since the concentrations in FRAP experiments are much lower (0.04 mg/ml), the peptides can be expected to be present in their monomer form.

Table 4. Hydrodynamic radii (r_h) of unlabelled and labelled peptides/proteins.

Peptide/protein	r_h unlabelled (nm)	r_h labelled (nm)
GK3	1.10	2.53
GK4	1.09	1.31
GK6	1.11	1.44
GK10	1.12	222
ZZA	2.50	2.42
HSA	2.51	2.68

At the studied conditions, CD spectra showed no difference between the labelled and the unlabelled equivalents of the peptides/proteins (Figure 9). The GK peptides displayed spectra typical for random coil, whereas Affibody molecules showed typical bands for alpha helical structures, and the mAb trastuzumab (Herceptin) showed signals corresponding to beta-sheet formations.

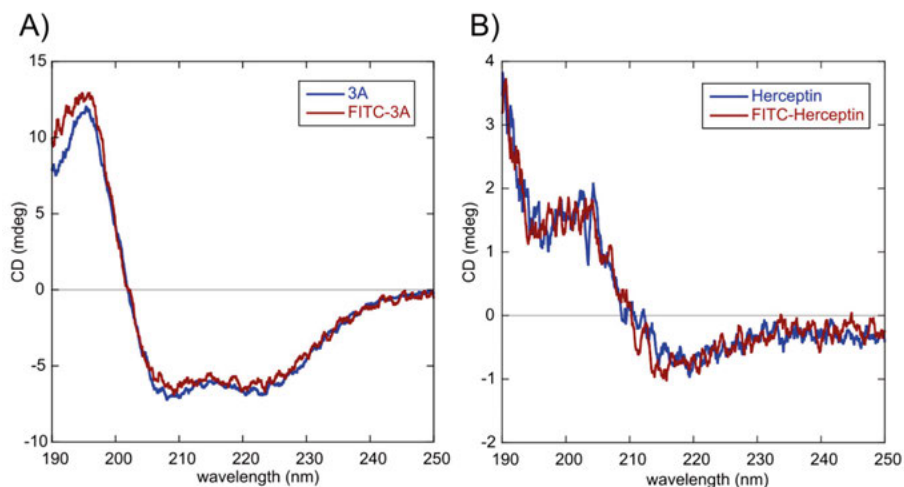


Figure 9. Representative CD-spectra showing typical signals for alpha helical structures for the Affibody molecule 3A (A) and characteristic bands for beta-sheets for Herceptin (B). No difference between FITC-labelled (red lines) and unlabelled (blue lines) equivalents of the proteins can be seen.

To conclude, the chemical conjugation of FITC to a small peptide can have a major impact on its overall physicochemical properties such as size, charge, hydrophobicity, and aggregation propensity. However, for larger proteins the labelling is likely not to affect their properties to the same extent. Nevertheless, the effect of labelling should be tested and discussed for each molecule individually and clear conclusions can only be drawn when comparing similar molecules with systematically varied properties.

Validation of the FRAP method

In order to validate the accuracy and robustness of the FRAP method, the self-diffusion coefficients of FD4 in PBS solutions with varying viscosities were determined and compared to values predicted from the Stokes-Einstein equation (eq. (4), Figure 10). Despite varying experimental conditions such as the size of the bleached ROI as well as the microscope used, the obtained values

were in agreement with the expected diffusion coefficients. However, it should be noted that diffusion coefficients larger than $80 \mu\text{m}^2/\text{s}$ were slightly overestimated. Hence, the FRAP method is especially suitable for quantitative determination of diffusivities of therapeutic proteins with $r_h > 2.7 \text{ nm}$ ($M_w > 25 \text{ kDa}$) and even for smaller peptides/proteins in the case of hindered diffusion within hydrogels.

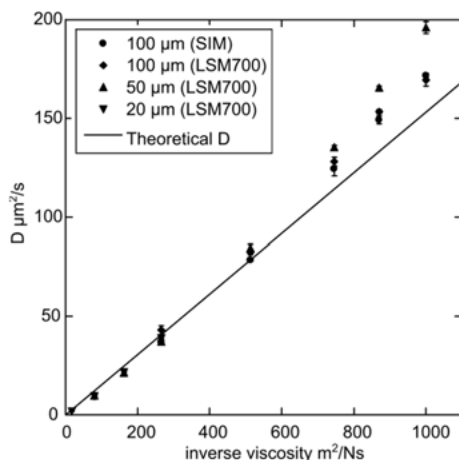


Figure 10. Diffusivities (D) of 4 kDa FITC-dextran in sucrose solutions of varying viscosities at $20 \text{ }^\circ\text{C}$ analysed with rFRAP using different spot sizes ($20 \mu\text{m}$, $50 \mu\text{m}$ or $100 \mu\text{m}$) and different microscopes (SIM or LSM700). The line represents theoretical diffusion coefficients calculated with the Stokes-Einstein equation (eq. (4)).

Hydrodynamic size

The hydrodynamic size of all tested compounds was determined with FRAP in PBS solution at the same concentrations as the subsequent experiments. For globular proteins, it has been shown that the hydrodynamic radius (r_h in nm) of the protein generally is related to its molecular weight (M_w in kDa) according to the following equation [67]:

$$r_h = 0.912M_w^{\frac{1}{3}} \quad (12)$$

For FITC-dextran (FD), the equivalent relation to estimate r_h is the following [57]:

$$r_h = 0.645Mw^{1/2} \quad (13)$$

In Figure 11, predictions of the hydrodynamic radii for globular proteins (eq. (12)) and FDs (eq. (13)) are shown, as well as the experimentally determined hydrodynamic radii of all tested model drugs. For small peptides/proteins ($Mw < 6$ kDa) and for FDs, the predictions are in good agreement with experimental data. FDs up to 70 kDa are in the size range relevant for therapeutic peptides/proteins and are therefore suitable model compounds. The hydrodynamic radius of FD150, on the other hand, is much larger than for mAbs of equivalent molecular weight (9.6 nm for FD150 compared to 5-6 nm for mAbs). Since the mesh size of most of the studied gels is in the range of 4-20 nm, FD150 cannot be expected to enter the gels to a large extent and is therefore excluded in the subsequent result sections.

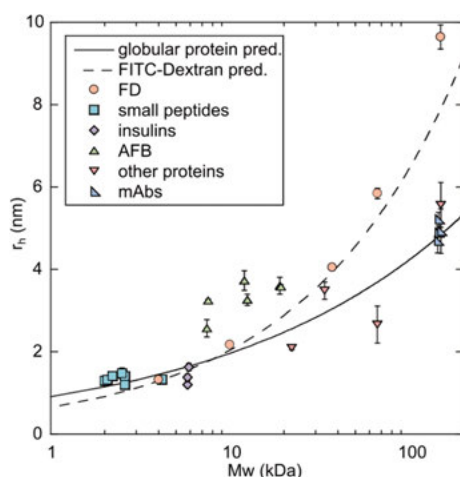


Figure 11. Hydrodynamic radius (r_h) of all tested compounds determined with FRAP in PBS solution. The lines represent predictions for globular proteins (eq. (12), solid) and FITC-dextran (eq. (13), dashed).

For larger proteins ($Mw > 7$ kDa), the experimentally determined values deviate from the predictions, indicating that their hydrodynamic size is affected by other factors in addition to molecular weight, such as shape, oligomerization, and glycosylation pattern. This was most pronounced for the Affibody molecules for which the experimentally determined hydrodynamic radii deviated considerably from the predictions. This can be partly attributed to their shape being rather ellipsoidal, as can be visualized from AlphaFold predictions (Figure 12A).

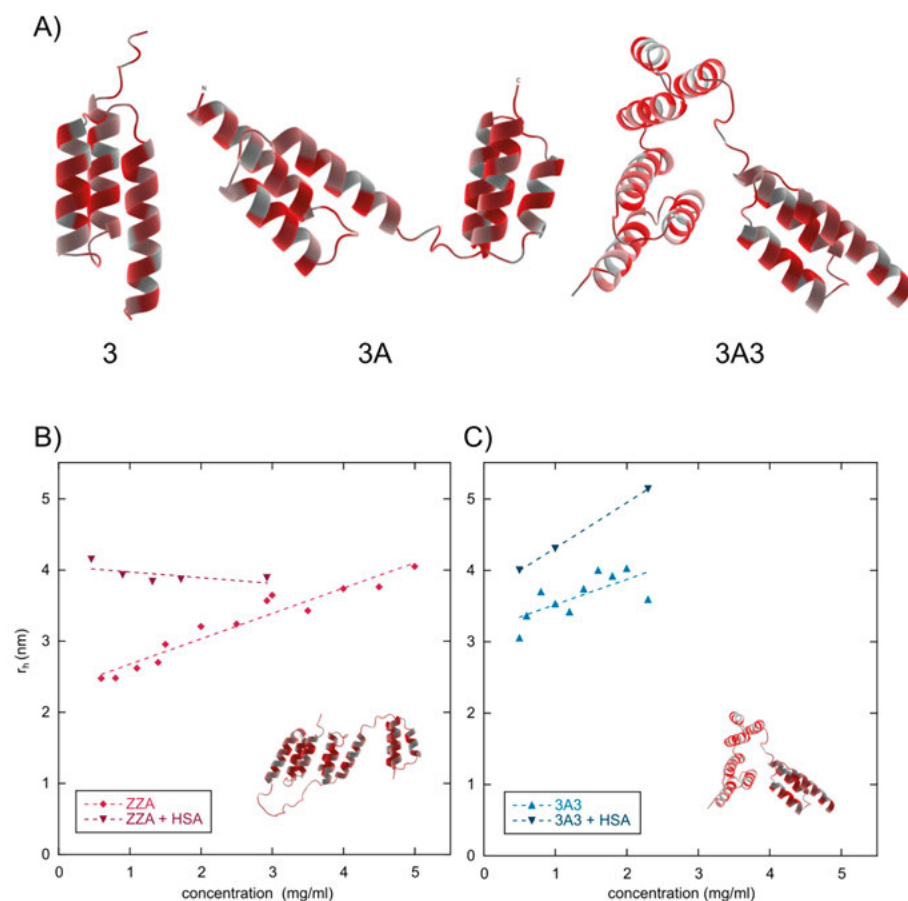


Figure 12. Structural visualization of Affibody molecules 3, 3A and 3A3 based on AlphaFold-predictions (A) and hydrodynamic radii (r_h) of Affibody molecules ZZA (B) and 3A3 (C) at different concentrations determined with FRAP in PBS solution with and without presence of 10 mg/ml unlabelled HSA.

However, merely the ellipsoidal shape is not sufficient to explain the apparently high hydrodynamic radii of the Affibody molecules. Evaluating the apparent hydrodynamic radii of Affibody molecules ZZA and 3A3 with FRAP at varying concentrations (Figure 12B, C), a clear trend of increasing size with increasing concentration is visible, indicating that concentration dependent reversible oligomerization may lead to the formation of complexes of larger size than Affibody monomers. When unlabelled HSA is present in the buffer solution, both ZZA and 3A3, which both contain a high-affinity ABD, appear larger ($r_h \approx 4$ nm), reflecting the size of the HSA-Affibody complex. Increasing the concentration of ZZA does not affect its apparent hydrodynamic radius in presence of HSA, whereas the apparent hydrodynamic radius of 3A3 increases with increasing concentration. This can be seen as an indication of the

formation of larger complexes composed of several HSA-Affibody entities. However, the size and identity of these complexes cannot be determined from diffusion measurements only.

Partitioning

The investigated model drugs were chosen to be able to enter the relatively loose gel network of the different gels via passive diffusion. After equilibration of the gels in solutions of the fluorescently labelled compounds, most of the gels were indistinguishable from the surrounding solution. Near neutral compounds of small to intermediate size distributed evenly between gel and solution, which can be seen in microscopy images of the gel-solution interface as low contrast between the different regions (Figure 13A).

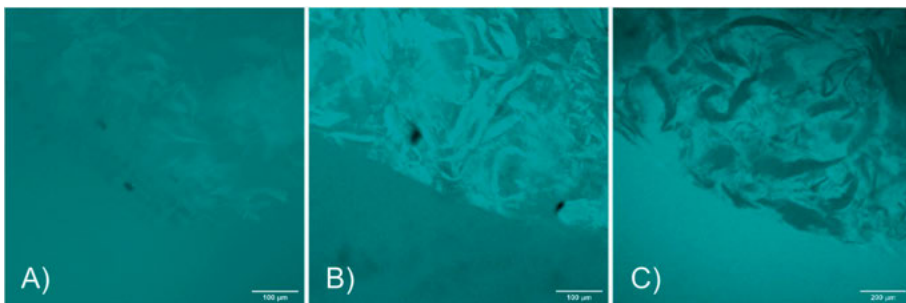


Figure 13. Confocal microscopy images (640x640 μm or 1280x1280 μm) of FITC-labelled Insulin aspart (A), denosumab (B) and etanercept (C) in COL-HA gels at the interface between gel and solution 100 μm into the gel. Insulin aspart is relatively evenly distributed within the gel, whereas denosumab is enriched in fibre-like structures and etanercept appears to be restricted from entering the polymer-rich domains.

Highly positively charged compounds were enriched in COL-HA and HA gels due to electrostatic interactions with the oppositely charged gel network. Interestingly, in COL-HA gels, structures of high intensity were visible adjacent to channels of similar intensity as the surrounding solution, indicating increased distribution to the polymer-rich regions of the gel (Figure 13B). For larger or highly negatively charged compounds, on the other hand, polymer-rich domains appeared as darker regions of the gel surrounded by channels of similar intensity as the surrounding solution (Figure 13C). This observation was quantified in terms of the partition coefficient (K), which was defined as the ratio of the mean fluorescence intensity within the gel and the mean fluorescence intensity in the surrounding solution.

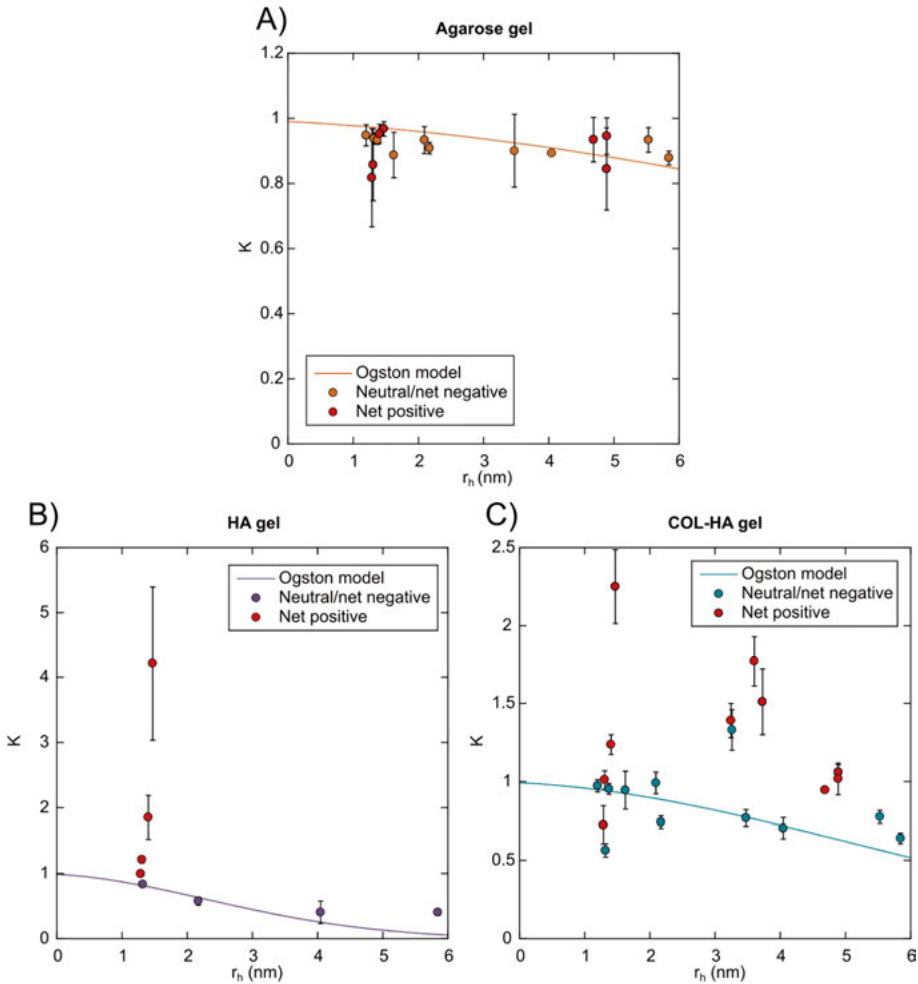


Figure 14. Partition coefficients (K) determined experimentally as the ratio of the fluorescence intensity within the gel and the surrounding solution for model drugs with varying hydrodynamic radius (r_h) in the different gel types A) agarose, B) hyaluronic acid (HA) and C) mixed collagen-hyaluronic acid (COL-HA). The lines represent predictions of K as a function of r_h calculated with the Ogston model (eq. (7)). Net positively charged compounds are highlighted in red.

In Figure 14, the experimentally determined partition coefficients are depicted in comparison to the Ogston model (eq. (7)). The data points in agarose gel are in good agreement with the theoretical model when assuming a mesh size of 20 nm. Considering HA and COL-HA gels, on the other hand, electrostatic interactions of the net positively charged compounds result in enrichment in the oppositely charged gels, which has to be described with a different theoretical model.

In Figure 15, the electrostatic PB model (eq. (8)) describing the contribution of electrostatic binding to the partition coefficients is visualized in comparison to experimental data. In order to highlight the electrostatic effects, the experimentally determined partition coefficients were divided by their respective obstruction factors determined with (eq. (7)), resulting in K_{PB} . Clearly, the model captures the trend of increased partitioning to HA gel and COL-HA gel depending on the net charge.

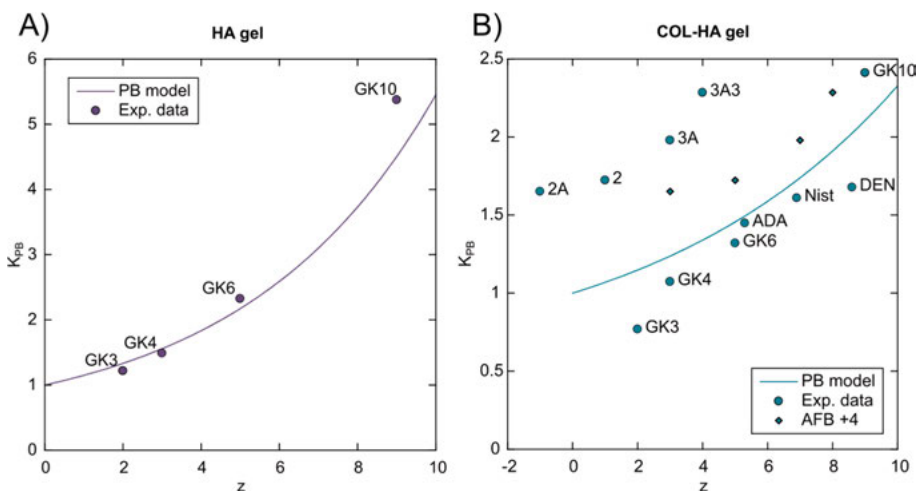


Figure 15. The contribution of electrostatic interactions to the partition coefficient (K_{PB}) in (A) hyaluronic acid gels (HA) and (B) mixed collagen-hyaluronic acid gels (COL-HA) as a function of the net charge (z) of the model drugs. The line represents the electrostatic peptide binding model (eq. (8)). Small diamonds correspond to Affibody molecules assuming +4 increased charge.

However, for the tested Affibody molecules, the calculated K_{PB} are slightly higher than predicted by the PB model (Figure 15B). There are several possible explanations for this. As discussed in the section about hydrodynamic size, there were clear signs of oligomerization of the Affibody molecules in solution. For calculation of the obstruction factor, the hydrodynamic radius determined in solution is used, which in the case of Affibody molecules reflects the size of the monomer-oligomer mixture present in solution. A shift of the monomer-oligomer equilibrium within the gel towards a larger extent of monomers with smaller hydrodynamic radii would imply an overestimated obstruction factor, which, to some extent, would explain the shift of the data points towards higher K_{PB} .

Additionally, oligomers present within the gel would be expected to have an increased overall apparent net charge of the complex compared to the assumed net charge of the monomer. Moreover, charge regulation in presence

of the oppositely charged polyelectrolyte can lead to increased apparent net surface charge of the complex macromolecules [68,69]. Assuming charge regulation to a net charge of +4 higher for all the Affibody molecules that were enriched in the gel provides a good fit with the theoretical model (small diamonds in Figure 15B).

Diffusion

Agarose gel

The diffusivity of a compound within the gel network relative to its diffusivity in solution ($D_{\text{gel}}/D_{\text{sol}}$) can be described by theoretical models as a function of its hydrodynamic size. In Figure 16, the obstruction model (eq. (9)) and the hydrodynamic model (eq. (10)) are visualized in comparison to experimental data from all projects included in this thesis. Both models are in fairly good agreement with experimental data for FDs, small peptides, other proteins and mAbs (Figure 16A).

The behaviour of the insulins and the Affibody molecules, on the other hand, are not well described by either of the models (Figure 16B). Interestingly, these are compounds for which the diffusion can be affected by their oligomerization state. Disturbance of the equilibrium of monomers, dimers, and oligomers in presence of the gel network would have a considerable impact on the relative diffusivity as it is normalized with the diffusivity in solution ($D_{\text{gel}}/D_{\text{sol}}$). Whereas the gel network appears to favour the monomer version of the Affibody molecules, leading to apparently increased $D_{\text{gel}}/D_{\text{sol}} > 1$, the insulins appear to be present in a higher oligomerization state when inside the gel leading to decreased diffusivities and $D_{\text{gel}}/D_{\text{sol}}$ lower than expected.

It can be concluded that both obstruction and hydrodynamic models work well to describe the diffusivities of a variety of differing macromolecules in neutral agarose gels, but the models are less suitable to predict the diffusivities of molecules that are prone to form oligomers. Moreover, measurements of diffusivities in hydrogels can give indications of macromolecules' oligomerization propensity in confined spaces.

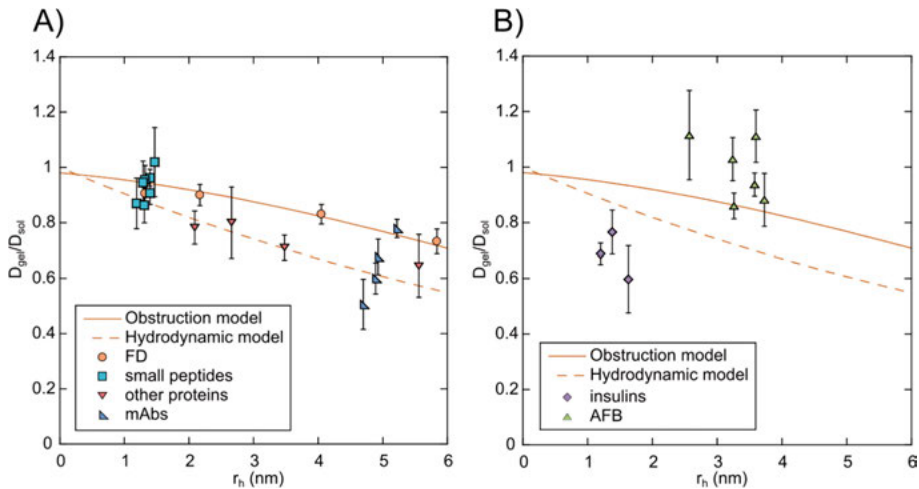


Figure 16. Normalized diffusivities (D_{gel}/D_{sol}) in Agarose gel in comparison to theoretical predictions calculated with the obstruction model (eq. (5)) or hydrodynamic model (eq. (10)). Experimental data for FDs, small peptides and mAbs are in good agreement with the models (A), whereas data for insulins and Affibody molecules deviate from the predictions (B).

HA-gel

Gels composed of 2% thiol-modified HA exhibit a homogeneous and relatively dense gel network with a mesh size of ~ 4.9 nm, so that only the subset of smaller compounds ($r_h < 4$ nm) is relevant for studies of diffusion within the gel. In Figure 17A, experimentally determined D_{gel}/D_{sol} for FDs and peptides with $r_h < 4$ nm are depicted as a function of their hydrodynamic radius in comparison to predictions of the obstruction model (eq. (9)) and the hydrodynamic model (eq. (10)). The models are in reasonable agreement with the experimental data for near-neutral compounds (net charge between -2 and +2).

The D_{gel}/D_{sol} of highly charged compounds, on the other hand, deviate considerably from the predictions, since electrostatic interactions in the highly charged HA gels play an important role for the diffusivities of charged peptides. In Figure 17B, the results are expressed as $(D_{gel}/D_{sol})_{PB}$, which is D_{gel}/D_{sol} divided by the obstruction factor according to eq. (9), in order to compensate for obstruction effects. The PB model (eq. (11)) describing the contribution of electrostatic interactions to the decrease in diffusivity for the positively charged compounds as a function of their net charge, is in good agreement with experimental data.

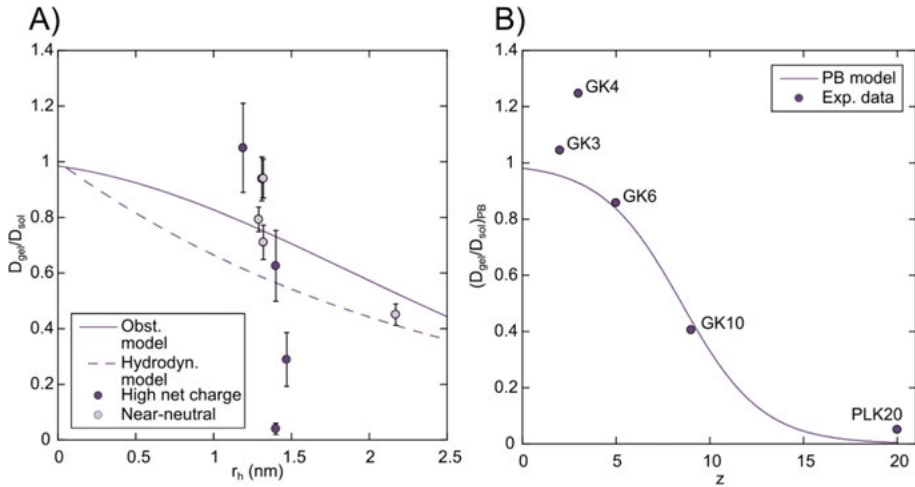


Figure 17. A) Normalized diffusivities (D_{gel}/D_{sol}) of small model compounds ($r_h < 4\text{nm}$) in HA gel as a function of their hydrodynamic radius (r_h). The lines represent theoretical D_{gel}/D_{sol} calculated with the obstruction model (eq. (9)) or hydrodynamic model (eq. (10)). Near-neutral compounds (net charge between -2 and +2) are highlighted in light purple. B) The contribution of electrostatic interactions to the normalized diffusivities ($(D_{gel}/D_{sol})_{PB}$) of positively charged peptides in HA gels. The line represents the electrostatic peptide binding model (eq. (11)).

Interestingly, also negatively charged compounds appear to be affected by electrostatic interactions with the gel network. The diffusivity of PLE20 (-20) and exenatide (-3) appeared to be increased in HA gels. The reason for that is not clear, but could be attributed to electrostatic repulsion of the HA chains effectively pushing the compounds to channels of low polymer concentration. Additional measurements of peptides with varying number of negative charges would be needed to develop and test the predictive ability of theoretical models describing the apparent increase of the diffusivities for negatively charged compounds. However, since the partitioning of highly negatively charged compounds to gels of the same charge is low, it is challenging to achieve a sufficient concentration of fluorescently labelled compounds within the gel to determine the diffusion coefficient with FRAP.

In conclusion, HA gels are suitable for investigation of electrostatic interactions of small compounds ($r_h < 4\text{ nm}$). The presented PB-model, in conjunction with the obstruction model, can be used to predict the decrease in the diffusivities for positively charged compounds in oppositely charged gels.

COL-HA gel

As can be seen in Figure 18, neither the obstruction model nor the hydrodynamic model is sufficient to describe the change in diffusivities in COL-HA

gels. In the complex environment that the hybrid gel network represents, other effects such as oligomerization, adsorption, size exclusion, and electrostatic interactions can affect the observed diffusivities. In the following, the obstruction model will be used to account for the contribution of hindered diffusion within the gel due to size effects.

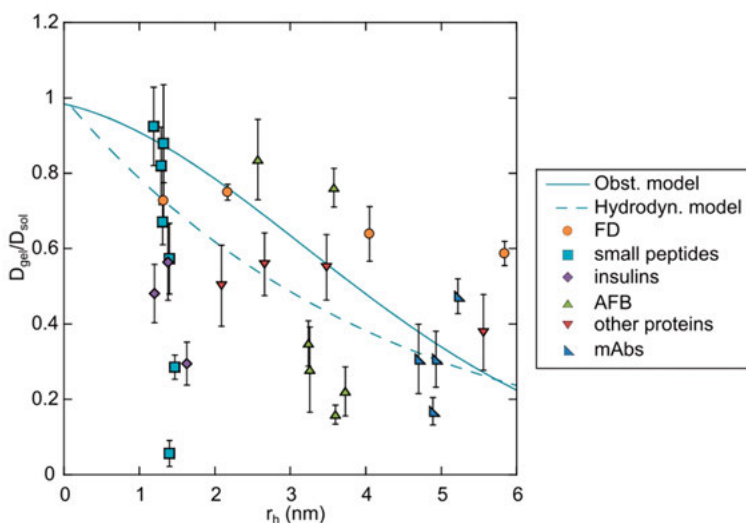


Figure 18. Normalized diffusivities ($D_{\text{gel}}/D_{\text{sol}}$) of all model compounds in COL-HA gel as a function of their hydrodynamic radius (r_h). The lines represent theoretical $D_{\text{gel}}/D_{\text{sol}}$ calculated with the obstruction model (eq. (9)) or hydrodynamic model (eq. (10)).

From microscopy images, it is evident that positively charged compounds tend to enrich in polymer-rich regions of the gel. Since the mesh size in these regions is narrower, the observed $D_{\text{gel}}/D_{\text{sol}}$ for compounds that are enriched in the gel ($K > 1$) is lower than expected from predictions with the obstruction model based on the average mesh size of the gel. Using the mesh size of the polymer-rich region instead provides closer agreement with experimental data (Figure 19A). For compounds with $K < 0.9$, on the other hand, $D_{\text{gel}}/D_{\text{sol}}$ is better described using the average mesh size of the gel. Compounds with $r_h > 4$ nm deviate from both curves as they appear to be distributed to the polymer-lean regions of the gel, where the diffusion is less restricted.

Thus, the uneven distribution between polymer-rich and polymer-lean regions can explain some of the observed trends. However, the large decrease of the diffusivities with increasing number of positive charges has to be explained by additional electrostatic effects. Figure 19B shows the experimental $D_{\text{gel}}/D_{\text{sol}}$ values, normalized by the respective obstruction factor according to eq. (9), to isolate the contribution of electrostatic interactions ($(D_{\text{gel}}/D_{\text{sol}})_{\text{PB}}$)

for compounds with $K > 1$. These data are compared with the predictions of the PB model (eq. (11)). For compounds with $r_h < 4\text{nm}$, the mesh size of the polymer-rich region was used, whereas for larger compounds the average mesh size of the gel was used for calculation of the obstruction factor. The model is in qualitative agreement with most of the experimental data, describing a sharp decrease in the diffusivities for compounds with a net charge above 5. Again, assuming the Affibody molecules to charge regulate to charges increased by 4, better agreement with the model is achieved (small diamonds in Figure 19B).

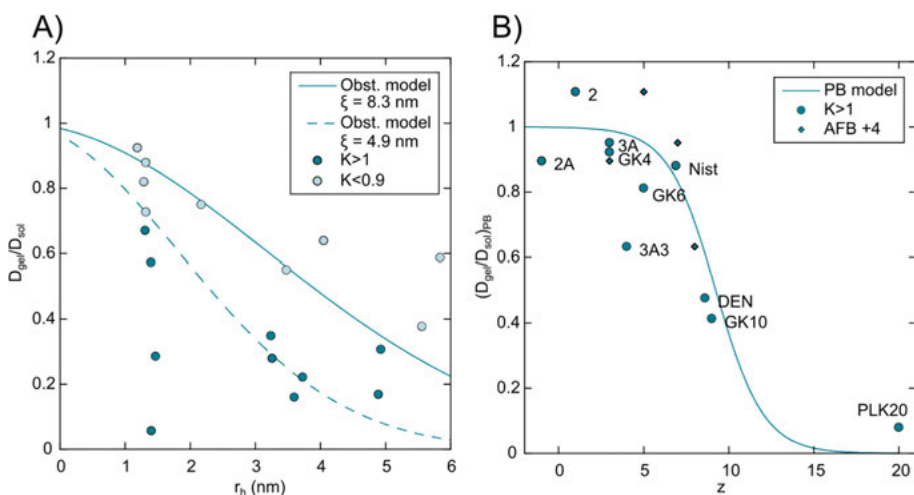


Figure 19. A) Normalized diffusivities (D_{gel}/D_{sol}) of model compounds enriched in the gel ($K > 1$) or depleted from the gel ($K < 0.9$) in COL-HA gel as a function of their hydrodynamic radius (r_h). The lines represent theoretical D_{gel}/D_{sol} calculated with the obstruction model (eq. (9)) using the average mesh size of the gel ($\xi = 8.3$ nm) or the mesh size in the polymer-rich regions of the gel ($\xi = 4.9$ nm). B) The contribution of electrostatic interactions to the normalized diffusivities $(D_{gel}/D_{sol})_{PB}$ of model drugs enriched in COL-HA gels ($K > 1$). The line represents the electrostatic peptide binding model (eq. (11)). Small diamonds correspond to Affibody molecules assuming +4 increased charge.

To conclude, the results demonstrate that the diffusivities of most of the tested model drugs in COL-HA gels were affected by their size and charge to an extent that can be quantified and predicted by theoretical models. However, for complex molecules, the apparent size and charge are not only determined by their molecular weight and net charge, but also by oligomerization and charge regulation processes. The presented *in vitro* method provides a tool to investigate these properties of drug candidates intended for SC injection.

Moreover, the distribution of the compounds between polymer-rich and polymer-lean domains within the gels also has an impact on the resulting

diffusivities of the model drugs. Due to the heterogeneous nature of the biological tissue, this is relevant in the context of ECM mimetic systems. Through qualitative analysis of microscopy images, this distribution can be assessed and considered, providing additional insights into the transport behaviour of different model drugs.

Effects of albumin presence

Apparent size

For Affibody molecules including a high affinity ABD, strong binding to HSA could be confirmed in solution and was clearly evident as a decrease of the diffusivity in presence of HSA (Figure 20). The resulting HSA-Affibody complex for Affibody molecules 3A and 3A3 had the same diffusivity as the full-size mAb Herceptin, indicating that presumably also larger complexes were present. The size and identity of the complexes, however, were not investigated in this work.

Interestingly, Affibody molecules 2 and 3, despite not containing an ABD, were also affected by the presence of HSA, but in the opposite direction, resulting in higher diffusivities in solution. This effect can be attributed to the solubilizing property of HSA [70], shifting the monomer-oligomer equilibrium of the Affibody molecules towards the monomer form.

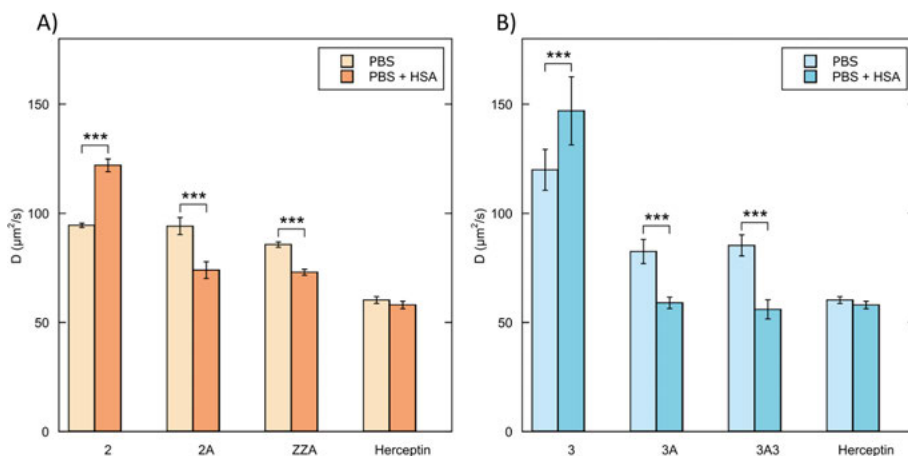


Figure 20. Experimentally determined diffusivities (D) of HER2-binders and ZZA (A) and HER3-binders and Herceptin (B). Statistically significant differences between measurements in PBS solution without (light columns) and with HSA (darker columns) are indicated (***, $p < 0.0001$).

Distribution within the gel

As discussed in the section about partitioning, some of the Affibody molecules (2A, 2, 3A and 3A3) were clearly enriched in COL-HA gels, showing regions of high intensity surrounded by regions of low intensity (Figure 21, upper row). When unlabelled HSA was present, the distribution of Affibody molecules containing an ABD was much more even within the gel (Figure 21, lower row). Binding to HSA appears to suppress the electrostatic binding of the Affibody molecules to the gel network, relocating the HSA-Affibody complex to the polymer-lean regions of the gel where the mesh size is larger.

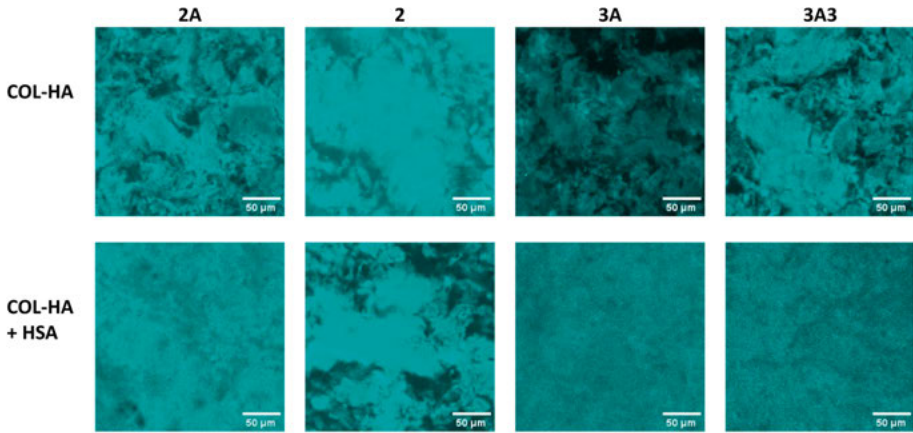


Figure 21. Microscopy images (246x246 μm) of FITC-labelled Affibody molecules 2A, 2, 3A and 3A3 in collagen-hyaluronic acid gels without (upper row) and with 10 mg/ml unlabelled HSA in the solution (lower row). Distinct structures of high intensity can be distinguished in absence of HSA, which are not present in presence of HSA with the exception of Affibody molecule 2 lacking ABD, for which the structures are even more pronounced in presence of HSA.

The shift towards polymer-lean regions of the gel results in increased $D_{\text{gel}}/D_{\text{sol}}$. However, since the size of the complex increases due to binding to HSA, the absolute diffusivity is also affected in the opposite direction. In the case of Affibody molecule 2A, the two opposing effects balance so that its diffusivity remains effectively unchanged (Figure 22), although binding to HSA is clearly evident from the changed distribution within gels. For the highly positively charged Affibody molecules 3A and 3A3, on the other hand, the redistribution and decreased electrostatic binding dominate. For these molecules, HSA effectively acts as a transporter, increasing the diffusivities in the gel.

For Affibody molecule 2, which does not include an ABD, the partitioning to the polymer-rich regions increased in presence of HSA (Figure 21). The reason for that is unclear, but it highlights the complex interplay between the

gel network, HSA, and the Affibody molecule with varying molecular design and physicochemical properties. The presented *in vitro* model can be a useful tool for systematic evaluation of these aspects, facilitating the development of new Affibody-based drugs with tuneable absorption properties.

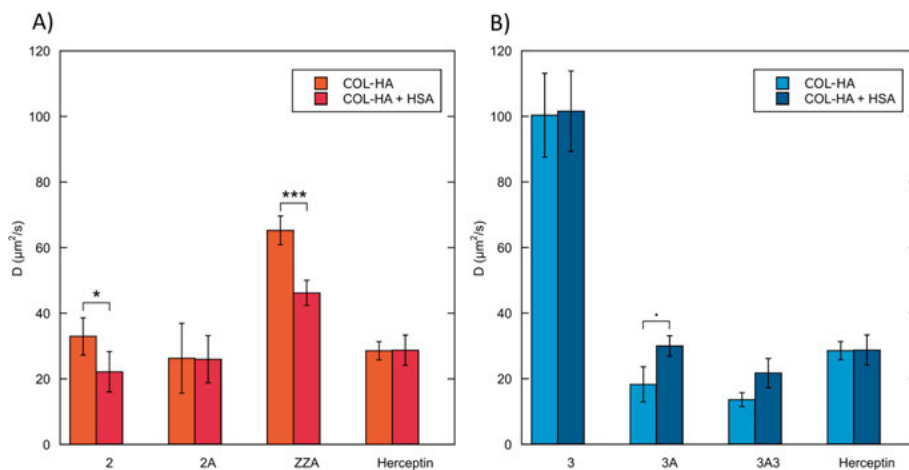


Figure 22. Experimentally determined diffusivities (D) of HER2-binders and ZZA (A) and HER3-binders and Herceptin (B) in COL-HA gel. Statistically significant differences between measurements in PBS solution without (light columns) and with HSA (darker columns) are indicated (***) $p < 0.0001$; *, $p < 0.01$; ·, $p < 0.05$).

Prediction of *in vivo* absorption rate

In project IV, the experimentally determined parameters (t_h , K , D) for eight therapeutic proteins intended for SC administration, were used to inform a PBPK model for the prediction of absorption rate and bioavailability after SC administration. In Figure 23, the time to achieve 90% of the maximum fraction absorbed as predicted from different runs of the PBPK model ($t_{90\%}$), is compared to t_{\max} reported in the literature. It should be noted that t_{\max} is not only affected by a compound's absorption kinetics but also by the elimination processes occurring during the absorption phase, whereas $t_{90\%}$ reflects merely the time to reach an arbitrarily chosen percentage of absorption. Although $t_{90\%}$ is not directly related to t_{\max} , both terms reflect the absorption rate and can be used to compare the rank order of the different compounds. The proteins were chosen to represent a wide range of absorption profiles, ranging from fast-acting insulin aspart with t_{\max} just below 1h, to the mAb denosumab for which the highest plasma concentration is reached after 10 days.

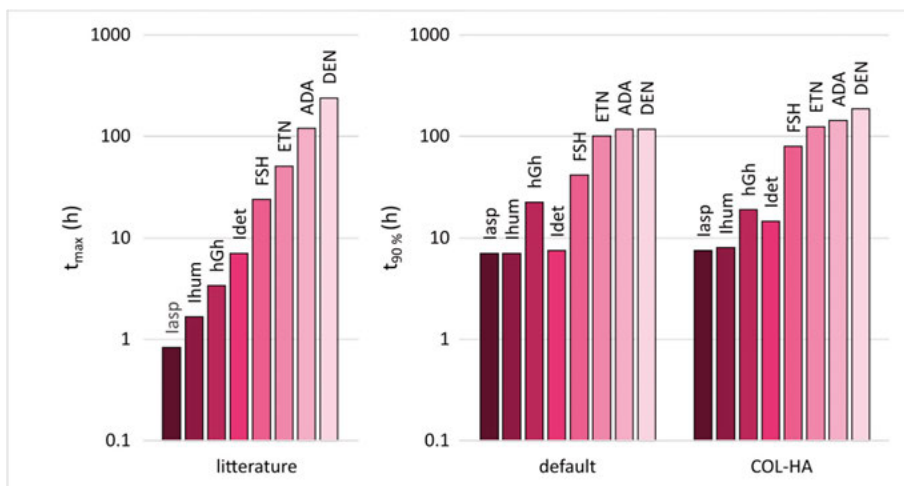


Figure 23. PBPK model predicted time to reach 90% absorption ($t_{90\%}$) using default settings or input from experiments COL-HA gels in comparison to t_{\max} from *in vivo* human pharmacokinetic data reported in the literature.

The PBPK model using the default settings (r_h predicted from Mw and D predicted for a globular protein) captures some of the differences in the absorption profile of the proteins. However, compounds of similar size, such as different insulin variants or different mAbs, cannot be distinguished. Using hydrodynamic radii and diffusion coefficients determined experimentally in PBS solution, improves the predictions of the model for the insulins for which oligomerization status is an important attribute. However, no difference in the model predictions for the mAbs could be observed. Adding the information of partition and diffusion coefficients in agarose gel does not improve the model further.

In contrast, informing the model with partition and diffusion coefficients in COL-HA gels contributes the additional information of electrostatic interactions, so that the rank order of absorption rates could be determined for all compounds, with the exception of insulin detemir. *In vivo*, the absorption rate after SC injection of insulin detemir is much lower than for the rapid-acting insulin analogues as a result of reversible HSA-binding leading to the formation of larger complexes. In the PBPK predictions, the difference between the insulins is much smaller, since the effect of HSA-binding was not considered in the model, and HSA was not present in the *in vitro* experiments. Indirectly, this is another indication of the importance to include HSA in *in vitro* models aiming to mimic the physiological environment.

Overall, it could be demonstrated that the experimental results determined in the presented *in vitro* setup can be used to improve the predictions of the PBPK model. Although quantitatively accurate predictions of t_{\max} are not

achieved at this point, the rank order of t_{\max} of a wide range of compounds could be predicted and differences in absorption rate of seemingly similar compounds could be detected. Therefore, systematic evaluation of drug candidates with varying properties using the presented *in vitro* method together with predictions of the pharmacokinetics with the PBPK model should be integral for the design and choice of drug candidates with optimized transport properties.

Main findings

Paper I

- ECM mimetic hydrogels are useful *in vitro* models for investigation of factors affecting drug transport after SC administration.
- COL-HA gels resemble a physiologically relevant environment in terms of network mesh size and interaction sites, and display good reproducibility and stability.
- FRAP is a reliable method for quantitative determination of local diffusivities (D) in solution and within gels.

Paper II

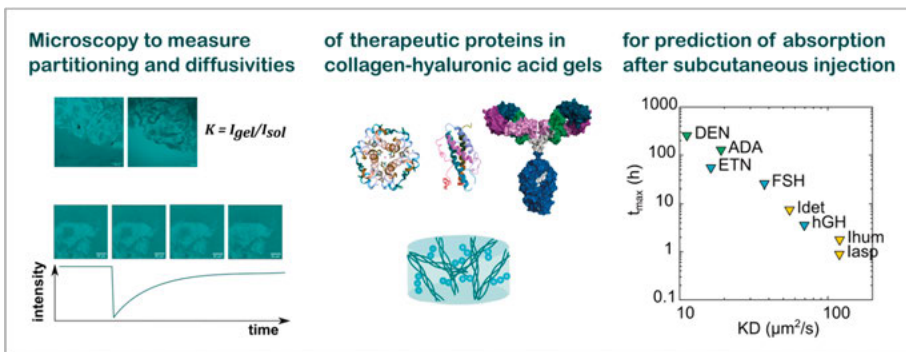
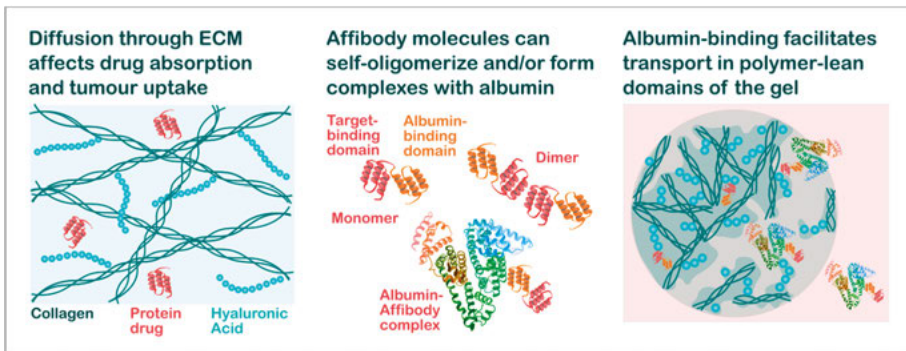
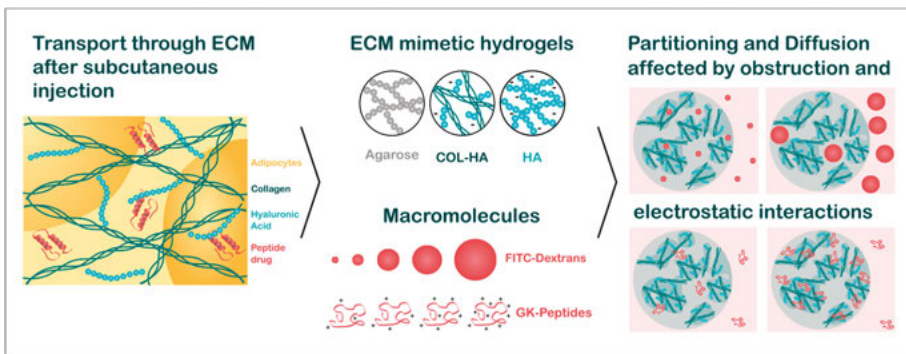
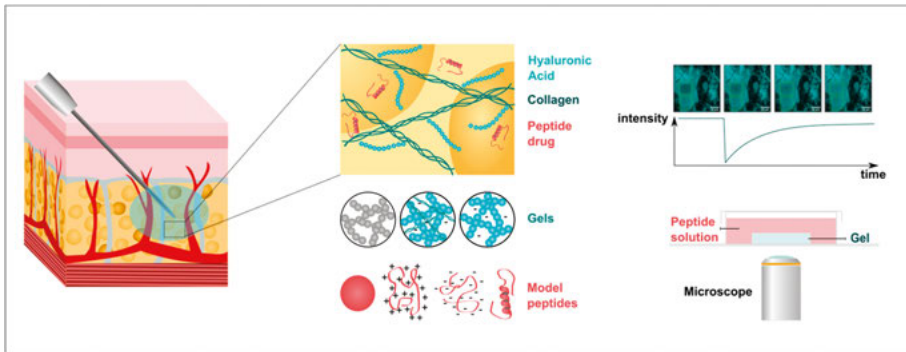
- Confocal microscopy can be used to determine partition coefficients (K) between gel and solution, and can reveal differences in distribution within heterogeneous gels.
- K and D of near-neutral compounds are generally decreased in the gels as a result of obstruction effects.
- Electrostatic interactions of cationic compounds in anionic gels lead to increased K accompanied by a decrease in D.
- Theoretical models (obstruction model and PB model) describe the effect of size and charge for a compound's K and D in hydrogels.

Paper III

- D of a protein in solution depends on its molecular weight, but also on its molecular shape and oligomerization state.
- D of cationic Affibody molecules in anionic gels decreased mostly as a result of increased distribution to denser polymer-rich regions.
- The presence of HSA changes D of Affibody molecules in solution and K and D in the gels, especially for molecules with an ABD.

Paper IV

- The combined information of K and D of a therapeutic protein in COL-HA gels is correlated to its absorption rate *in vivo*.
- The experimental data can be used to improve PBPK model predictions of the absorption rate.



Concluding remarks and future perspectives

In recent years, there have been increased efforts to create and evaluate physiologically relevant *in vitro* models in order to understand mechanisms affecting the absorption rate and bioavailability of subcutaneously administered drug compounds. Many of these focus on studies of mass transfer of a drug compound from a donor compartment representing the injected depot, through a medium serving as a mimic of the ECM of the tissue, into an acceptor compartment reflecting blood or lymphatic absorption.

The *in vitro* method presented in this thesis is based on confocal laser scanning microscopy and FRAP, which enables the visualization and quantification of interactions with the gel matrix in terms of partition and self-diffusion coefficients at equilibrium instead. Although the necessity of fluorescent labelling is a considerable limitation of the method, the possibility to visualize interactions with the heterogeneous gel matrix and the need for small amounts of material, make this microscopy-based method a valuable tool to gain insights into the mechanisms affecting drug transport through hydrogels.

The hydrogels that were found to be most suitable as a mimetic of the ECM were COL-HA gels composed of the most abundant biopolymers in the tissue at physiologically relevant concentrations, forming a heterogeneous network enabling the investigation of obstruction effects, size-exclusion, and electrostatic interactions.

Another component present in the ECM that has been included in the model in project III, is albumin (HSA), which appears to play an intricate role in the absorption behaviour of drug compounds. HSA offers many specific and non-specific binding sites, and the transport of molecules can be affected by the presence of HSA in various ways. Some of these mechanisms were studied in this work, but more efforts are needed to evaluate the relative contributions of the different mechanisms to the total observed absorption and biodistribution profile of a drug with binding affinity to HSA. Understanding and finetuning the albumin-binding properties of a compound can be important for new extended-release formulations, as many interesting drug compounds employing this principle are emerging on the market, such as GLP-1 analogues and insulin variants.

Despite efforts to include the most relevant interaction sites, none of the currently available SC *in vitro* models has been able to capture all relevant factors affecting the absorption rate and bioavailability of a compound on its own. Models can be improved by including additional components present in the ECM or by changing the absolute and relative composition of the polymers to more accurately mimic the microstructure of the tissue.

However, more complicated models do not necessarily provide more mechanistic insight, and therefore, simple models should be preferable to elucidate the individual contributions of different mechanisms. Therefore, a set of complementary methods answering to different aspects of the absorption process informing *in silico* models integrating the combined information derived from these parameters into physiologically relevant predictions, would be the most preferable strategy to reach reliable predictions of absorption rate and bioavailability of new drug candidates.

For that purpose, simple *in vitro* models characterizing the transport behaviour of a drug compound as an intrinsic property, with the need for only small amounts of material, such as the described methods, should be an integrated part of the profiling of new candidates. This would help to choose and design drug candidates with a favourable predicted pharmacokinetic profile at an early stage of drug development, before moving on to preclinical studies. Well-informed choice of candidates for preclinical studies can in turn decrease the number of animal experiments needed.

Moreover, increased understanding of mechanisms affecting the transport of drug molecules through the ECM can also be valuable to refine strategies to improve tumour tissue penetration or inspire new modified release formulations. Ultimately, the method presented in this thesis can be useful as a characterization tool for new drug candidates, leading to mechanistic insight for improved molecular design of drug compounds with a predictable PK profile, eventually facilitating the development of new effective drugs to diagnose, treat, and cure diseases.

Populärvetenskaplig sammanfattning

Biologiska läkemedel är en stor grupp mediciner, som inkluderar bland annat insulin för behandling av diabetes, GLP-1-läkemedel för vikttnedgång, hormoner som används vid fertilitetsbehandling och vissa målsökande cancerläkemedel. De kan oftast inte tas som tabletter eftersom de bryts ner i magen. Därför sprutas de istället in subkutan, det vill säga under huden, ofta med hjälp av enkla injektionspennor som patienter kan använda själva.

När läkemedlet hamnat under huden måste det ta sig genom vävnaden och in i blod- eller lymfkärlen. Hur snabbt detta går beror på hur läkemedelsmolekylerna rör sig i den så kallade extracellulära matrisen – ett vätskefyllt nätverk av bland annat kollagen, hyaluronsyra och proteiner. Små molekyler rör sig snabbt och tas lätt upp i blodet, medan större molekyler rör sig långsammare och följer lymfflödet i större utsträckning. Upptaget kan också påverkas om molekylerna klumpar ihop sig eller binder till de olika beståndsdelar i vävnaden.

För att utveckla nya läkemedel behöver man veta hur snabbt och hur mycket som tas upp i kroppen efter en injektion. Det är svårt att förutsäga detta endast utifrån fysikalkemiska egenskaper, datormodeller eller djurförsök, som ofta inte stämmer överens med resultat hos människor. Det saknas också bra standardiserade tester i laboratoriemiljö, så kallade *in vitro* metoder.

I denna avhandling användes därför särskilda geler av kollagen och hyaluronsyra för att efterlikna miljön under huden. Med mikroskopi och FRAP-metodik mättes hur olika molekyler spreds och rörde sig i gelen. Studierna visade att storlek, laddning och bindning till proteiner som albumin kraftigt påverkar hur läkemedel transporteras i gelen.

I ett senare steg jämfördes resultaten från *in vitro* försöken med hur vissa godkända läkemedel faktiskt tas upp hos människor. Diffusions- och fördelningsdata från experimenten kunde förklara generella skillnader i absorptions-hastighet, särskilt när de kombinerades med datormodeller.

Sammanfattningsvis har arbetet gett ökad förståelse för hur biologiska läkemedel rör sig i kroppen efter en subkutan injektion. Metoden kan hjälpa till att bedöma nya läkemedelskandidater och göra det lättare att förutsäga hur de kommer att fungera hos patienter.

Populärwissenschaftliche Zusammenfassung

Biologische Arzneimittel umfassen eine große Gruppe moderner Medikamente. Dazu gehören unter anderem Insulin zur Behandlung von Diabetes, GLP-1-Wirkstoffe zur Gewichtsreduktion, Hormone für Fertilitätsbehandlungen sowie zielgerichtete Krebsmedikamente. Da diese Wirkstoffe im Magen abgebaut werden, können sie nicht als Tabletten eingenommen werden. Stattdessen werden sie subkutan, also unter die Haut, injiziert.

Nach der Injektion müssen die Moleküle durch das Gewebe in Blut- oder Lymphgefäße gelangen. Dafür bewegen sie sich durch die extrazelluläre Matrix, ein flüssigkeitsgefülltes Netzwerk aus unter anderem Kollagen, Hyaluronsäure und Proteinen. Kleine Moleküle diffundieren relativ schnell und gelangen rasch ins Blut. Größere Moleküle sind langsamer und folgen häufig dem Lymphfluss. Der Transport kann zusätzlich beeinträchtigt werden, wenn Moleküle zusammenlagern oder an Bestandteile des Gewebes binden.

Für die Entwicklung neuer subkutaner Arzneimittel ist es entscheidend, die Aufnahmegeschwindigkeit und -menge zuverlässig vorhersagen zu können. Physikochemische Daten, Computermodelle oder Tierversuche reichen dafür jedoch oft nicht aus, da die Ergebnisse häufig nicht mit den Daten im Menschen übereinstimmen. Außerdem gibt es bisher keine gut etablierten Labortests, die den Transport durch menschliches Gewebe realistisch nachstellen können.

In dieser Arbeit wurden speziell entwickelte Gele aus Kollagen und Hyaluronsäure eingesetzt, um die Umgebung unter der Haut zu simulieren. Mithilfe von Mikroskopie und FRAP-Messungen wurde untersucht, wie sich verschiedene Modellmoleküle im Gel verteilen und bewegen. Die Ergebnisse zeigten, dass Größe, elektrische Ladung und die Bindung an Proteine wie Albumin den Transport im Gel klar beeinflussen.

Zuletzt wurden die Laborergebnisse mit bekannten Aufnahmedaten von bereits zugelassenen Protein-Arzneimitteln beim Menschen verglichen. Die gemessenen Diffusions- und Verteilungswerte konnten allgemeine Unterschiede in der Absorptionsgeschwindigkeit erklären, vor allem in Kombination mit Computermodellen. Insgesamt trägt die Arbeit dazu bei, die Transportmechanismen biologischer Arzneimittel nach einer subkutanen Injektion besser zu verstehen und neue Wirkstoffe zuverlässiger zu bewerten.

Acknowledgements

This book is the result of a journey that lasted a little over seven years—years filled with PhD courses, conferences, teaching course lab close to 100 days, a pandemic, two rounds of parental leave, experiments that worked and many that didn't, numerous pong sessions, journal clubs, writing clubs, a move to a new department and corridor, and countless hours in the dark microscopy room. Here I would like to acknowledge all the people who made this possible and enjoyable.

The work in this doctoral thesis was carried out at the Department of Pharmacy and the Department of Medicinal Chemistry, both at the Faculty of Pharmacy, Uppsala University. The project was part of the Swedish Drug Delivery Center SweDeliver and was financially supported by a combination of industrial partners, Vinnova and Uppsala University.

The supervisors

First of all, I would like to thank my main supervisor, **Per**, for offering me the opportunity to pursue a PhD in his research group. The generous, supportive, and relaxed environment in the group—where the research question always comes first and where I was given maximum freedom to shape my own project—has been invaluable. It took some time to adapt, but this independence helped me grow into a more confident researcher, and in the end, I truly enjoyed taking full responsibility for my work. Thank you for your trust, and for your endless interest and patience in discussing physical chemistry and explaining difficult equations.

Helen, you have made a real difference for me. Your industry perspective, combined with your deep knowledge of drug delivery and peptide and protein therapeutics, were the ideal complement to this work. Thank you for always making time for my questions, even when you were very busy. I always valued our regular supervisor meetings—sharing new results, exploring early interpretations, and the genuine enthusiasm, encouragement, constructive feedback you brought to every discussion.

I would also like to thank my co-supervisor, **Magnus**, for being available whenever guidance was needed, even if only occasionally. I am also grateful to my former co-supervisor, **Jette**, who contributed valuable input during the early stages of the work before moving on to new responsibilities.

The Collaborators

Thanks to the collaborators at **AstraZeneca**, who provided interesting model compounds already at the start of the project. But most of all so much knowledge and expertise in all the WP1 meetings in discussions about the future of the project. I am truly grateful for our collaboration with **Affibody**. **Anna, Åsa, Ida, Fredrik, Rezan**: you not just provided the perfect molecules for Project III—you also brought genuine scientific curiosity and were always so friendly, helpful, and enthusiastic in all our exchanges. Thanks also to **Fering** for providing some of the proteins for project IV adding completely new interesting questions to the project. **Erik**, we had talked about collaborating since the early days of SweDeliver, and I am glad we finally made it happen in the last project. Thank you for your flexibility, for answering all my questions about the PBPK model, and for running simulations so quickly.

Reviewers

Thank you to the anonymous reviewers. Whoever you are, your feedback and input really improved the quality of the published papers, although it was very scary to receive the first really critical comments. I am very grateful for the scientific community and to be part of it.

BioVis staff

Thank you for introducing me to the fascinating world of microscopy, image analysis, and the beauty of false colours. I spent many hours in the dark microscopy room learning to master the settings, and I am especially grateful to **Jeremy**, who often stopped by to offer technical support, discuss unexpected results, or simply check in on how things were going.

Degree project students

Teaching really is the best way to learn. Thank you to all my students both at course lab and at the research lab for your clever questions and for pushing me to explain physical chemistry in new ways. My degree project students **Ali, Eva, Nadia, Rawan, Pontus**: being part of your final project and watching you become more independent and design your own experiments has been truly rewarding. I am especially happy that some of our joint work made it into the publications so you could be acknowledged for your hard work.

FFK group

Thank you all for your support and for discussions and input at our group meetings, journal clubs and seminars. Thank you, **Johan**, for explaining the FRAP equations again and again, and for your help to include relevant statistics in the papers. **Agnes**, you taught me all about the gels and were such a kind and friendly office mate. Thanks to **Lina** and **Randi**, for introducing me to the PhD student life, and the available methods in the group. Thanks to all of you post-docs and researchers: **Sean, Anna, Franz, Enamul, Jonas, David, Victor**. Even if some of you were here just for a short time, you came in with new inspiration and ideas. Thanks also to **Sana**, whose behind-the-scenes efforts—from ordering materials to managing teaching and cleaning schedules—kept everything running smoothly.

Big thank you to my fellow PhD students in the group: **Yassir, Marcus, Vahid, Ellen, Anton, Rojita, Giorgia**. It has been a pleasure to walk by your side in this journey, to teach and learn together, celebrate each other's success and support each other when things did not go that well. **Ellen**, having you as my office mate these past years has meant so much to me. We first met when you were a pharmacy student in our group, and now you have not only caught up but will even finish before me. You are genuinely a remarkable person—full of enthusiasm, curiosity, and humour. I loved how you would stop by in the lab, genuinely interested in whatever experiments were going on. I really enjoyed our shared unit-work and writing club; we got so much work done, and most importantly it was so much more fun together.

Pongsters

Sohan, Irès, Aleksei, Shakhawath, Jamal, Tomas, Rosita, Marilena: You gave me the warmest welcome I could have hoped for. In those early days, when everything felt so confusing, it was such a relief to just play ping-pong and laugh until my stomach hurt. It has been amazing to be surrounded by such wonderful, nerdy people who know how to have fun and don't take everything too seriously.

SweDeliver and SweDeliver people

Maryam, Anna, Nicklas, Marco, Prosper, Yuming, Benyamin, Martin, Vicky, Ilse, Rebekkah, Jonas, Lidia, Xiguo, Shahina, Hannah, Caroline: it has been a privilege to join workshops, seminars, thesis defences, summits, and retreats with you, and to be updated on the latest research in drug delivery—even in areas far from my own work. Seeing the bigger picture and taking part in high-level discussions was truly inspiring, giving me a deeper understanding of the broader challenges in Swedish drug delivery. A special

thank you to the mentoring program and to my mentor, **Cecilie**, who during the mentoring year helped me recognize my comfort zones and gently encouraged me to step beyond them.

Corridor neighbours

Oliver, Fredrik, Katarina, Lars, Philipp, Luis, Said, Wahida: Thank you for the joint drug-delivery seminars—a forum where we could regularly practice our presentation skills and dive deep into ongoing research. **Malin, Jenny, Emelie, Nichlas, and Janis:** Thank you for spreading so much joy and energy in our corridor. **Fanny and Lovisa:** My “gå-din-termin” buddies—thank you for helping me find structure amid the chaos of deadlines and ambitions. **Anton, Esther, Marcus, Andrea, and Ulrika:** Thank you for your help with LC–MS and for always being available for a chat when I was roaming the corridors. This list could go on much longer, because I had the privilege of being surrounded by so many amazing, funny, curious, open, and warm people. I always felt welcome across the entire Faculty of Pharmacy.

The people who make the department work

Warm thanks to the administrative staff, **Heléne, Pernilla** and **Anette** at the department of Pharmacy and **Birgitta, Catrin, Sandra** and **Regina** at Medicinal Chemistry, and the heads of the departments over the years, **Erik, Anders** and **Mikael**, for creating a good work environment for the PhD students and truly “a great place to work at”.

But there is more to life than just work – believe it or not. I would like to thank family and friends, who helped me remember that even in the most stressful times.

Gruvfolkskören

Even though—or maybe precisely because—we never talk about work, you have meant so much to me during the making of this book and for keeping me from going a little crazy along the way. Singing with you and learning new pieces has been such a joy, and it is so absorbing that it truly demands all my focus. That is exactly what makes it the perfect way to recharge and find balance.

The family...

... in Germany

Mama, thank you for always listening to my endless explanations of fascinating drug delivery systems and biological drugs—and for asking genuinely interested questions. Your support has meant so much to me. You were a true

inspiration, showing me that it is possible to study and even change professions while raising two small children. I still remember reading about basic natural science in your physiotherapy books for the first time and being completely fascinated. I would also like to thank my brother, **Robert**, who first sparked my interest in chemistry and shared countless fun and nerdy discussions about science with me, that continue to inspire me today.

... who have left us

I would also have loved to share this final product of the past years with my **Omi**, who was always my greatest supporter and a wonderful inspiration—teaching me to be humble, curious, and playful in learning. At special occasions like this, I miss **my father** a lot. I remember him patiently explaining logarithms to me during one of our running sessions, and I would have loved to share this thesis with him and hear his thoughts. Though he is no longer here, his curiosity, humour, and love of learning continue to inspire me every day.

... in law

I am so grateful to my parents in law, **Steffi** and **Thomas**, who are such an amazing support as they have realized that “Zeit statt Zeug” is the most appreciated gift for parents. Thanks for all the times you showed up and took care of the girls, which allowed me to travel and go to conferences.

... who I share my everyday life with

My beloved husband **Hannes**, who is the reason I moved to Sweden and without whom much of this would not have happened. Thank you for your support, for listening to me and agreeing with me so often, but also for being honest and direct when it is actually I who should pull myself together. **Linnea** and **Majken**, my wonderful daughters, I love you more than anything, and it is such a joy to watch you grow and develop. I genuinely wish for you to find a project as rewarding and fulfilling as this one has been for me, be it within science or in any other field. Thanks to the three of you, and our joyful dog, I have been nudged out of my own head and into the forest to play or make things. And time and again, that has ended up being the best way to find solutions.

Finally, to everyone who crossed my path during these years—thank you. This thesis may have my name on the cover, but it carries a little piece of each of you.

References

- [1] H.M. Kinnunen, R.J. Msrny, Improving the outcomes of biopharmaceutical delivery via the subcutaneous route by understanding the chemical, physical and physiological properties of the subcutaneous injection site, *J. Control. Release* 182 (2014) 22–32. <https://doi.org/10.1016/j.jconrel.2014.03.011>.
- [2] M.R. Turner, S. V. Balu-Iyer, Challenges and Opportunities for the Subcutaneous Delivery of Therapeutic Proteins, *J. Pharm. Sci.* 107 (2018) 1247–1260. <https://doi.org/10.1016/j.xphs.2018.01.007>.
- [3] H.M. Kinnunen, V. Sharma, L.R. Contreras-Rojas, Y. Yu, C. Alleman, A. Sreedhara, S. Fischer, L. Khawli, S.T. Yohe, D. Bumbaca, T.W. Patapoff, A.L. Daugherty, R.J. Msrny, A novel in vitro method to model the fate of subcutaneously administered biopharmaceuticals and associated formulation components., *J. Control. Release* 214 (2015) 94–102. <https://doi.org/10.1016/j.jconrel.2015.07.016>.
- [4] W.F. Richter, S.G. Bhansali, M.E. Morris, Mechanistic determinants of biotherapeutics absorption following SC administration, *AAPS J.* 14 (2012) 559–570. <https://doi.org/10.1208/s12248-012-9367-0>.
- [5] I.R. Dubbelboer, E. Sjögren, Physiological based pharmacokinetic and biopharmaceutics modelling of subcutaneously administered compounds – An overview of in silico models, *Int. J. Pharm.* 621 (2022) 121808. <https://doi.org/10.1016/J.IJPHARM.2022.121808>.
- [6] A. Datta-Mannan, S. Estwick, C. Zhou, H. Choi, N.E. Douglass, D.R. Witcher, J. Lu, C. Beidler, R. Millican, Influence of physiochemical properties on the subcutaneous absorption and bioavailability of monoclonal antibodies, *MAbs* 12 (2020). <https://doi.org/10.1080/19420862.2020.1770028>.
- [7] I. Nakajima, T. Yamaguchi, K. Ozutsumi, H. Aso, Adipose tissue extracellular matrix: newly organized by adipocytes during differentiation, *Differentiation* 63 (1998) 193–200. <https://doi.org/10.1111/J.1432-0436.1998.00193.X>.
- [8] E.C.M. Mariman, P. Wang, Adipocyte extracellular matrix composition, dynamics and role in obesity, *Cell. Mol. Life Sci.* 67 (2010) 1277–1292. <https://doi.org/10.1007/S00018-010-0263-4>.
- [9] P. BJÖRNTORP, A. MARTINSSON, The Composition of Human Subcutaneous Adipose Tissue in Relation to Its Morphology, *Acta Med. Scand.* 179 (1966) 475–481. <https://doi.org/10.1111/J.0954-6820.1966.TB05485.X>.
- [10] M. Thomsen, M. Poulsen, M. Bech, A. Velroyen, J. Herzen, F. Beckmann, R. Feidenhans, F. Pfeiffer, Visualization of subcutaneous insulin injections by x-ray computed tomography, *Phys. Med. Biol.* 57 (2012) 7191. <https://doi.org/10.1088/0031-9155/57/21/7191>.
- [11] A.S. Avram, M.M. Avram, W.D. James, Subcutaneous fat in normal and diseased states: 2. Anatomy and physiology of white and brown adipose tissue, *J. Am. Acad. Dermatol.* 53 (2005) 671–683. <https://doi.org/10.1016/J.JAAD.2005.05.015>.

- [12] D.S. Collins, L.C. Kourtis, N.R. Thyagarajapuram, R. Sirkar, S. Kapur, M.W. Harrison, D.J. Bryan, G.B. Jones, J.M. Wright, Optimizing the Bioavailability of Subcutaneously Administered Biotherapeutics Through Mechanochemical Drivers, *Pharm. Res.* 34 (2017) 2000–2011. <https://doi.org/10.1007/S11095-017-2229-9>.
- [13] R.K. Reed, S. Lepsoe, H. Wiig, Interstitial exclusion of albumin in rat dermis and subcutis in over- and dehydration, *Am. J. Physiol. - Hear. Circ. Physiol.* 257 (1989). <https://doi.org/10.1152/ajpheart.1989.257.6.h1819>.
- [14] H. Wiig, M.A. Swartz, Interstitial fluid and lymph formation and transport: Physiological regulation and roles in inflammation and cancer, *Physiol. Rev.* 92 (2012) 1005–1060. <https://doi.org/10.1152/physrev.00037.2011>.
- [15] Y. Zhu, I.L. Kruglikov, Y. Akgul, P.E. Scherer, Hyaluronan in adipogenesis, adipose tissue physiology and systemic metabolism, *Matrix Biol.* 78–79 (2019) 284–291. <https://doi.org/10.1016/j.matbio.2018.02.012>.
- [16] M. Ellmerer, L. Schaupp, G.A. Brunner, G. Sendlhofer, A. Wutte, P. Wach, T.R. Pieber, Measurement of interstitial albumin in human skeletal muscle and adipose tissue by open-flow microperfusion, *Am. J. Physiol. - Endocrinol. Metab.* 278 (2000). <https://doi.org/10.1152/ajpendo.2000.278.2.e352>.
- [17] P. Kurtzhals, S. Havelund, I. Jonassen, B. Kiehr, U.D. Larsen, U. Ribel, J. Markussen, Albumin binding of insulins acylated with fatty acids: characterization of the ligand-protein interaction and correlation between binding affinity and timing of the insulin effect in vivo, *Biochem. J.* 312 (1995) 725. <https://doi.org/10.1042/BJ3120725>.
- [18] D. Sleep, J. Cameron, L.R. Evans, Albumin as a versatile platform for drug half-life extension, *Biochim. Biophys. Acta* 1830 (2013) 5526–5534. <https://doi.org/10.1016/J.BBAGEN.2013.04.023>.
- [19] P. Descargues, E. Pagès, C. Jarret, Ex vivo subcutaneous injection model (Patent Application Publication (10) Pub . No . : US 2020/0400652 A1), 2020.
- [20] H.K. Bown, C. Bonn, S. Yohe, D.B. Yadav, T.W. Patapoff, A. Daugherty, R.J. Msrny, In vitro model for predicting bioavailability of subcutaneously injected monoclonal antibodies., *J. Control. Release* 273 (2018) 13–20. <https://doi.org/10.1016/j.jconrel.2018.01.015>.
- [21] M. Wanselius, S. Abrahmsén-Alami, B.I. Hanafy, M. Mazza, P. Hansson, A microfluidic in vitro method predicting the fate of peptide drugs after subcutaneous administration, *Int. J. Pharm.* 667 (2024). <https://doi.org/10.1016/J.IJPHARM.2024.124849>.
- [22] C. Gomes, K. Gridley, I. Anastasiou, B. Sinkó, R.J. Msrny, Hydrogel formats to model potential drug interactions occurring at the subcutaneous injection site, *Eur. J. Pharm. Biopharm.* 199 (2024) 114308. <https://doi.org/10.1016/J.EJPB.2024.114308>.
- [23] M.H. Hakim, B.H. Jun, A. Ahmadzadegan, P.M. Babiak, Q. Xu, K.P. Buno, J.C. Liu, A.M. Ardekani, P.P. Vlachos, L. Solorio, Investigation of macromolecular transport through tunable collagen hyaluronic acid matrices, *Colloids Surfaces B Biointerfaces* 222 (2023) 113123. <https://doi.org/10.1016/J.COLSURFB.2023.113123>.
- [24] T.A. Schöner, V. Vogel, M. Venczel, K. Knoth, W. Kamm, T. Paehler, G. Louit, I.T. Terán, P. Mundinger, A. Marker, P. Loos, M. Hittinger, C.M. Lehr, Biorelevant subcutaneous in vitro test predicts the release of human and fast acting insulin formulations, *Int. J. Pharm.* 655 (2024). <https://doi.org/10.1016/J.IJPHARM.2024.123995>.

- [25] D. Li, Q. Qin, A.A. Benetti, L. Kahouadji, M.G. Wacker, BioJect: An in vitro platform to explore release dynamics of peptides in subcutaneous drug delivery, *J. Control. Release* 380 (2025) 1058–1079. <https://doi.org/10.1016/J.JCONREL.2025.02.013>.
- [26] D.H. Leung, Y. Kapoor, C. Alleyne, E. Walsh, A. Leithead, B. Habulihaz, G.M. Salituro, A. Bak, T. Rhodes, Development of a Convenient In Vitro Gel Diffusion Model for Predicting the In Vivo Performance of Subcutaneous Parenteral Formulations of Large and Small Molecules, *AAPS PharmSciTech* 18 (2017) 2203–2213. <https://doi.org/10.1208/s12249-016-0698-5>.
- [27] S.S. Jensen, H. Jensen, C. Cornett, E.H. Møller, J. Østergaard, Real-time UV imaging identifies the role of pH in insulin dissolution behavior in hydrogel-based subcutaneous tissue surrogate, *Eur. J. Pharm. Sci.* 69 (2015) 26–36. <https://doi.org/10.1016/j.ejps.2014.12.015>.
- [28] F. Bock, E. Lin, C. Larsen, H. Jensen, K. Huus, S.W. Larsen, J. Østergaard, Towards in vitro in vivo correlation for modified release subcutaneously administered insulins, *Eur. J. Pharm. Sci.* 145 (2020) 105239. <https://doi.org/10.1016/j.ejps.2020.105239>.
- [29] I. Torres-Terán, M. Venczel, S. Klein, Prediction of subcutaneous drug absorption - Development of novel simulated interstitial fluid media for predictive subcutaneous in vitro assays, *Int. J. Pharm.* 658 (2024). <https://doi.org/10.1016/J.IJPHARM.2024.124227>.
- [30] A.M. Ledo, G. Misiewicz, T. Dimke, W.R. Tschantz, J. Handel, R. Pelis, G. Bruin, K. Bechtold-peters, M. Sanchez-felix, S. Deshmukh, Lab on a Chip Utility of an in vitro lymphatics on-chip model for monoclonal antibodies †, (2025). <https://doi.org/10.1039/d4lc00988f>.
- [31] C. Niederalt, L. Kuepfer, J. Solodenko, T. Eissing, H.U. Siegmund, M. Block, S. Willmann, J. Lippert, A generic whole body physiologically based pharmacokinetic model for therapeutic proteins in PK-Sim, *J. Pharmacokinet. Pharmacodyn.* 45 (2018) 235–257. <https://doi.org/10.1007/S10928-017-9559-4/TABLES/7>.
- [32] S. Benamara, C. Troisi, F. Gattacceca, E. Sjögren, L. Nguyen, D. Teutonico, Cross-Species Extrapolation of Neonatal Fc Receptor (FcRn) Binding Affinity to Predict Monoclonal Antibody Pharmacokinetics in Humans Using Physiologically Based Pharmacokinetic Modeling (PBPK): Are We There Yet?, *ACS Pharmacol. Transl. Sci.* (2025). <https://doi.org/10.1021/ACSPTSCI.5C00356>.
- [33] B.I. Hanafy, I. Trayton, M. Sundqvist, J. Caldwell, N. Mody, K. Day, M. Mazza, Predicting human subcutaneous bioavailability of monoclonal antibodies using an integrated in-vitro/in-silico approach, *J. Control. Release* 380 (2025) 715–724. <https://doi.org/10.1016/J.JCONREL.2025.02.022>.
- [34] C. Bender, S. Eichling, L. Franzen, V. Herzog, L.M. Ickenstein, D. Jere, L. Nonis, G. Schwach, P. Stoll, M. Venczel, S. Zenk, Evaluation of In Vitro Tools to Predict the In Vivo Absorption of Biopharmaceuticals Following Subcutaneous Administration, *J. Pharm. Sci.* 111 (2022) 2514–2524. <https://doi.org/10.1016/J.XPHS.2022.04.005>.
- [35] Sáanuel, M. Burknchez-Félix, Me, H.H. Chen, C. Patterson, S. Mittal, Predicting bioavailability of monoclonal antibodies after subcutaneous administration: Open innovation challenge, *Adv. Drug Deliv. Rev.* (2020). <https://doi.org/10.1016/j.addr.2020.05.009>.
- [36] A. Rodler, A. Samanta, W.-J. Goh, J. Hilborn, P. Hansson, Engineering and characterization of a hydrogel mimicking subcutaneous interstitial space, (n.d.) 1–39.

- [37] S.R. Chary, R.K. Jain, Direct measurement of interstitial convection and diffusion of albumin in normal and neoplastic tissues by fluorescence photobleaching, *Proc. Natl. Acad. Sci. U. S. A.* 86 (1989) 5385–5389. <https://doi.org/10.1073/pnas.86.14.5385>.
- [38] G. Alexandrakis, E.B. Brown, R.T. Tong, T.D. McKee, R.B. Campbell, Y. Boucher, R.K. Jain, Two-photon fluorescence correlation microscopy reveals the two-phase nature of transport in tumors, *Nat. Med.* 10 (2004) 203–207. <https://doi.org/10.1038/nm981>.
- [39] A.C. Guyton, K. Scheel, D. Murphree, Interstitial fluid pressure. 3. Its effect on resistance to tissue fluid mobility., *Circ. Res.* 19 (1966) 412–419. <https://doi.org/10.1161/01.RES.19.2.412>.
- [40] N. Lorén, M. Nydén, A.M. Hermansson, Determination of local diffusion properties in heterogeneous biomaterials, *Adv. Colloid Interface Sci.* 150 (2009) 5–15. <https://doi.org/10.1016/j.cis.2009.05.004>.
- [41] N. Lorén, J. Hagman, J.K. Jonasson, H. Deschout, D. Bernin, F. Cella-Zanacchi, A. Diaspro, J.G. McNally, M. Ameloot, N. Smisdom, M. Nydén, A.M. Hermansson, M. Rudemo, K. Braeckmans, Fluorescence recovery after photobleaching in material and life sciences: Putting theory into practice, *Q. Rev. Biophys.* 48 (2015) 323–387. <https://doi.org/10.1017/S0033583515000013>.
- [42] D. Axelrod, D.E. Koppel, J. Schlessinger, E. Elson, W.W. Webb, Mobility measurement by analysis of fluorescence photobleaching recovery kinetics., *Biophys. J.* 16 (1976) 1055. [https://doi.org/10.1016/S0006-3495\(76\)85755-4](https://doi.org/10.1016/S0006-3495(76)85755-4).
- [43] R. Peters, J. Peters, K.H. Tews, W. Bähr, A microfluorimetric study of translational diffusion in erythrocyte membranes, *Biochim. Biophys. Acta - Biomembr.* 367 (1974) 282–294. [https://doi.org/10.1016/0005-2736\(74\)90085-6](https://doi.org/10.1016/0005-2736(74)90085-6).
- [44] H.G. Kapitza, G. McGregor, K.A. Jacobson, Direct measurement of lateral transport in membranes by using time-resolved spatial photometry., *Proc. Natl. Acad. Sci. U. S. A.* 82 (1985) 4122. <https://doi.org/10.1073/PNAS.82.12.4122>.
- [45] D.M. Soumpasis, Theoretical analysis of fluorescence photobleaching recovery experiments, *Biophys. J.* 41 (1983) 95–97. [https://doi.org/10.1016/S0006-3495\(83\)84410-5](https://doi.org/10.1016/S0006-3495(83)84410-5).
- [46] H. Deschout, J. Hagman, S. Fransson, J. Jonasson, M. Rudemo, N. Lorén, K. Braeckmans, Straightforward FRAP for quantitative diffusion measurements with a laser scanning microscope, *Opt. Express* 18 (2010) 22886–22905. <https://doi.org/10.1364/oe.18.022886>.
- [47] X.Z. Shu, Y. Liu, Y. Luo, M.C. Roberts, G.D. Prestwich, Disulfide cross-linked hyaluronan hydrogels, *Biomacromolecules* 3 (2002) 1304–1311. <https://doi.org/10.1021/bm025603c>.
- [48] G.L. Ellman, A colorimetric method for determining low concentrations of mercaptans, *Arch. Biochem. Biophys.* 74 (1958) 443–450. [https://doi.org/10.1016/0003-9861\(58\)90014-6](https://doi.org/10.1016/0003-9861(58)90014-6).
- [49] R. Ravichandran, M.M. Islam, E.I. Alarcon, A. Samanta, S. Wang, P. Lundström, J. Hilborn, M. Griffith, J. Phopase, Functionalised type-I collagen as a hydrogel building block for bio-orthogonal tissue engineering applications, *J. Mater. Chem. B* 4 (2015) 318–326. <https://doi.org/10.1039/c5tb02035b>.
- [50] W.A. Bubnis, C.M. Ofner, The determination of ϵ -amino groups in soluble and poorly soluble proteinaceous materials by a spectrophotometric method using trinitrobenzenesulfonic acid, *Anal. Biochem.* 207 (1992) 129–133. [https://doi.org/10.1016/0003-2697\(92\)90513-7](https://doi.org/10.1016/0003-2697(92)90513-7).

- [51] D.P. Nair, M. Podgórski, S. Chatani, T. Gong, W. Xi, C.R. Fenoli, C.N. Bowman, The Thiol-Michael addition click reaction: A powerful and widely used tool in materials chemistry, *Chem. Mater.* 26 (2014) 724–744. https://doi.org/10.1021/CM402180T/ASSET/IMAGES/LARGE/CM-2013-02180T_0024.JPEG.
- [52] J. Karvinen, T.O. Ihalainen, M.T. Calejo, I. Jönkkäri, M. Kellomäki, Characterization of the microstructure of hydrazone crosslinked polysaccharide-based hydrogels through rheological and diffusion studies, *Mater. Sci. Eng. C* 94 (2019) 1056–1066. <https://doi.org/10.1016/j.msec.2018.10.048>.
- [53] D. Shah, Y. Guo, J. Ocampo, J. Shao, FITC labeling of human insulin and transport of FITC-insulin conjugates through MDCK cell monolayer, *J. Pharm. Anal.* 9 (2019) 400–405. <https://doi.org/10.1016/j.jpha.2019.08.002>.
- [54] B. Giebel, C. Helmbrecht, Methods to analyze EVs, *Methods Mol. Biol.* 1545 (2017) 1–20. https://doi.org/10.1007/978-1-4939-6728-5_1/FIGURES/6.
- [55] MICROTRAC MRB, Dynamic Light Scattering: DLS Particle Analyzer :: Microtrac, Dyn. Light Scatt. Part. Size Zeta Potential Anal. (2021). <https://www.microtrac.com/products/dynamic-light-scattering/> (accessed November 24, 2025).
- [56] J. Schindelin, I. Arganda-Carreras, E. Frise, V. Kaynig, M. Longair, T. Pietzsch, S. Preibisch, C. Rueden, S. Saalfeld, B. Schmid, J.Y. Tinevez, D.J. White, V. Hartenstein, K. Eliceiri, P. Tomancak, A. Cardona, Fiji: An open-source platform for biological-image analysis, *Nat. Methods* 9 (2012) 676–682. <https://doi.org/10.1038/nmeth.2019>.
- [57] B.G. Amsden, Hydrogel Mesh Size and Its Impact on Predictions of Mathematical Models of the Solute Diffusion Coefficient, 45 (2022) 43. <https://doi.org/10.1021/acs.macromol.2c01443>.
- [58] J. Parlow, E. Pet, A. Smirnova, E. Mojumdar, H. Sjögren, P. Hansson, Diffusion of macromolecules in extracellular matrix mimetic hydrogels – effect of size and charge, *Eur. J. Pharm. Sci.* 214 (2025) 107257. <https://doi.org/10.1016/J.EJPS.2025.107257>.
- [59] A.G. Ogston, The spaces in a uniform random suspension of fibres, *Trans. Faraday Soc.* 54 (1958) 1754–1757.
- [60] E.M. Johnson, D.A. Berk, R.K. Jain, W.M. Deen, Diffusion and partitioning of proteins in charged agarose gels, *Biophys. J.* 68 (1995) 1561–1568. [https://doi.org/10.1016/S0006-3495\(95\)80328-0](https://doi.org/10.1016/S0006-3495(95)80328-0).
- [61] B. Jönsson, Computer program written by Bengt Jönsson, (1998).
- [62] B. Amsden, An Obstruction-Scaling Model for Diffusion in Homogeneous Hydrogels, (1999). <https://doi.org/10.1021/ma980922a>.
- [63] R.I. Cukier, Diffusion of Brownian spheres in semidilute polymer solutions, *Macromolecules* 17 (1984) 252–255. <https://doi.org/10.1021/MA00132A023>.
- [64] T. Fujiyabu, X. Li, U. Il Chung, T. Sakai, Diffusion Behavior of Water Molecules in Hydrogels with Controlled Network Structure, *Macromolecules* 52 (2019) 1923–1929. <https://doi.org/10.1021/ACS.MACROMOL.8B02488>.
- [65] I. Nestorov, Whole body pharmacokinetic models, *Clin. Pharmacokinet.* 42 (2003) 883–908. <https://doi.org/10.2165/00003088-200342100-00002>.
- [66] B. Rippe, B. Haraldsson, Transport of macromolecules across microvascular walls: the two-pore theory, <https://doi.org/10.1152/Physrev.1994.74.1.163> (1994) 163–219. <https://doi.org/10.1152/PHYSREV.1994.74.1.163>.
- [67] M.M. Schmidt, K.D. Wittrup, A modeling analysis of the effects of molecular size and binding affinity on tumor targeting, *Mol. Cancer Ther.* 8 (2009) 2861–2871. <https://doi.org/10.1158/1535-7163.MCT-09-0195>.

- [68] D. Beyer, C. Holm, Z.G. Wang, Charge Regulation Effects in Weak Polyelectrolyte Complexation, *J. Phys. Chem. Lett.* 16 (2025) 8245–8251. <https://doi.org/10.1021/ACS.JPCLETT.5C01877>/ASSET/IMAGES/LARGE/JZ5C01877_0006.JPEG.
- [69] M. Lund, B. Jönsson, On the charge regulation of proteins, *Biochemistry* 44 (2005) 5722–5727. <https://doi.org/10.1021/BI047630O>/ASSET/IMAGES/LARGE/BI047630OF00006.JPEG.
- [70] E. Tarelli, A. Mire-Sluis, H.A. Tivnann, B. Bolgiano, D.T. Crane, C. Gee, X. Lemercinier, M.L. Athayde, N. Sutcliffe, P.H. Corran, B. Rafferty, Recombinant Human Albumin as a Stabilizer for Biological Materials and for the Preparation of International Reference Reagents, *Biologicals* 26 (1998) 331–346. <https://doi.org/10.1006/BIOL.1998.0163>.

Acta Universitatis Upsaliensis

Digital Comprehensive Summaries of Uppsala Dissertations from the Faculty of Pharmacy 395

Editor: The Dean of the Faculty of Pharmacy

A doctoral dissertation from the Faculty of Pharmacy, Uppsala University, is usually a summary of a number of papers. A few copies of the complete dissertation are kept at major Swedish research libraries, while the summary alone is distributed internationally through the series Digital Comprehensive Summaries of Uppsala Dissertations from the Faculty of Pharmacy. (Prior to January, 2005, the series was published under the title “Comprehensive Summaries of Uppsala Dissertations from the Faculty of Pharmacy”.)

